Modeling of Litz-Wire DD Coil With Ferrite Core for Wireless Power Transfer System

Min Wu, Xu Yang, *Senior Member, IEEE*, Hongchang Cui, *Graduate Student Member, IEEE*, Wenjie Chen, *Senior Member, IEEE*, Laili Wang, *Senior Member, IEEE*, Lei Zhu, *Graduate Student Member, IEEE*, Xipei Yu, and Zhengchao Yan, *Member, IEEE*

***Abstract*—DD planar coil with ferrite core is one popular coupling structure in wireless power transfer (WPT), especially for electric vehicle applications. The coil design is critical for improving the performance of WPT system. However, the coupler design purely relying on finite element analysis (FEA) software is time-consuming. Literature on the modeling of DD coil is lacking. Therefore, the model of DD coil with a ferrite core for calculating self-inductance, mutual inductance, and ac resistance is proposed in this article. The condition when primary and secondary coils have different sizes is also considered. The case that there is misalignment is also analyzed. Meanwhile, a genetic algorithm based on the proposed coil mathematical model is proposed to optimize the coil structure. For verifying the accuracy of the proposed model, the simulation model based on the FEA and a 1.2-kW laboratory prototype are built simultaneously. The calculation values based on the proposed model is highly consistent with the simulation results and experimental values. Error for calculating self-inductance and mutual inductance is within 5% when coils on the primary side and secondary side are in alignment. The error for calculating the ac resistance of the coil is within 10% when the frequency range is 0–200 kHz.**

***Index Terms*—AC resistance, analytical model, DD coil, genetic algorithm, mutual inductance, self-inductance, wireless power transfer (WPT).**

I. Introduction

WIRELESS power transfer is increasingly popular for its safety and convenience compared with the conventional plug-in charging method [1], [2], [3], [4], [5], [6], [7]. Applying wireless power transfer (WPT) to electric vehicles (EVs) for wireless charging is one of the most promising applications.

Manuscript received 19 May 2022; revised 14 September 2022; accepted 29 October 2022. Date of publication 24 November 2022; date of current version 10 March 2023. This work was supported in part by the National Natural Science Foundation of China under Grant 52201405, in part by the China Postdoctoral Science Foundation under Grant 2020TQ0237 and Grant 2021M702555, in part by the Power Electronics Science and Education Development Program of Delta Group, and in part by HPCPlatform, Xi'an Jiaotong University. Recommended for publication by Associate Editor R. Hui. *(Corresponding authors: Xu Yang.)*

Min Wu, Xu Yang, Hongchang Cui, Wenjie Chen, Laili Wang, Lei Zhu, and Zhengchao Yan are with the State Key Laboratory of Electrical Insulation and Power Equipment, Xi'an Jiaotong University, Xi'an 710049, China (e-mail: wm3117079009@stu.xjtu.edu.cn; yangxu@mail.xjtu.edu.cn; chc121@stu.xjtu.edu.cn; cwj@xjtu.edu.cn; llwang@mail.xjtu.edu.cn; jasmine@stu.xjtu.edu.cn; yanzc1991@gmail.com).

Xipei Yu is with the Center for Power Electronics Systems, Virginia Tech, Blacksburg, VA USA (e-mail: yxp19990719@vt.edu).

Color versions of one or more figures in this article are available at https://doi.org/10.1109/TPEL.2022.3222228.

Digital Object Identifier 10.1109/TPEL.2022.3222228

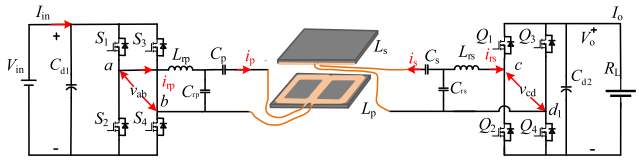

Fig. 1. A typical WPT system for the EV.

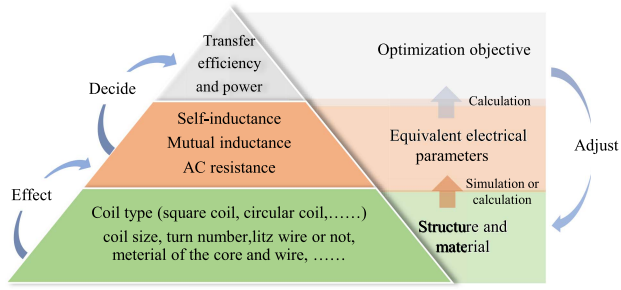

Fig. 2. Typical coil design process.

The magnetic coupler is a central part of the WPT system. The DD coil is proposed for the first time [8]. The DD coil consists of two single coils connected in series in the opposite direction. The single coil is usually rectangular spiral coil. It has been analyzed that the DD coil has better coupling performance and lower leakage flux compared with other coil structure [8], [9], [10]. Therefore, the DD coil has been widely used especially in the EV's application [11], [12], [13], [14], [15]. In practical applications, the DD coil is usually covered with a magnetic core for improving the coupling and magnetic shield, as shown in Fig.1.

A good design of coil is very critical for improving the performance of the WPT system. The strong power transfer capacity and high transfer efficiency are usually the objectives of coil design, which involves three variables: self-inductance, mutual inductance, and the ac resistance of the coupler, as shown in Fig. 2.

Generally, the coil is optimized to obtain the desired self-inductance and mutual inductance, as well as smaller resistance with the help of finite element analysis (FEA) software. However, there are some short comings related to this method. 1) The simulation model needs a large number of meshes in order to ensure the accuracy of simulation result.

Especially when Litz wire is adopted in the coil design, the simulation meshes will become enormous. 2) In order to find an optimized coil solution, large amount of coil models with different parameters need to be swept. Therefore, coil design that relies purely on simulation is very time-consuming. On the contrary, with the help of a mathematical model and intelligent algorithms, it becomes possible to design the coil quickly and accurately. Besides, the theoretical model of the coupler can help designers better understand the working principle of coupling mechanism and avoid some unnecessary try and error.

For calculating the self-inductance and mutual inductance, many works have been conducted, which can be classified into the following three categories.

1) Mathematical model is reported for the coreless coil in [16], [17], [18], [19], [20], [21], [22], [23], and [24]. In these models, the case that coil with ferrite is not considered. The coil structure is mainly single coil structure, such as circular coil and rectangular coil.
2) A method of calculating the self-inductance and mutual inductance of the circular coil or rectangular coil with ferrite was reported in [25], [26], [27], [28], and [29]. For models in [25] and [26], the magnetic core needs to be much larger than the coil area; otherwise, it leads to a great error. In [27], [28], and [29], the effect caused by the ferrite is considered. However, it is only applicable to spiral tubes with specific magnetic core structure
3) Several methods are introduced to calculate the inductance of the transformer [9], [30], [31], [32], [33]. In these cases, the winding is wrapped by the magnetic core and the magnetic leakage is very small. For reducing the ac resistance of the coil, the Litz wire is commonly used.

The key to calculate the ac resistance of the coil is to obtain the field distribution of the cross section of the Litz wire. The method for gaining the field distribution can be classified into two categories. 1) Field distribution is obtained by the analytical model [34], [35], [36], [37], [38], [39], [40], [41]. 2) Field distribution is obtained by the simulation [42], [43], [34], [35], [36] that put forward a method for analyzing the ac resistance of the circular coil. In these models, the ac resistance is calculated based on the assumption that the magnetic field magnitude is independent of the position at the circumferential direction in cylindrical coordinates, which is not valid for square coils or DD coils. Several models for calculating winding ac resistance were reported in [38], [39], [40], and [41]. In these models, the magnetic distribution is considered to be the same. However, this assumption is not valid for the planar coils.

In general, these existing literature mainly focus on the single circular, square coils, or the transformer winding. There is a lack of modeling for the DD planar coil with ferrite for calculating the self-inductance, mutual inductance, and ac resistance. Therefore, a mathematical model is proposed for calculating the self-inductance, mutual inductance, and ac resistance of the DD coil with the ferrite core in this article. Besides, a genetic algorithm based on the proposed coil mathematical model is proposed to optimize the coil structure. The main contributions are listed as follows.

1) A mathematical model of rectangular DD coil with ferrite core for calculating the inductance and mutual inductance is proposed. For calculating the inductance, the rectangular DD coil is divided into multiple straight segments. The self-inductance of each segment is calculated separately. The mutual inductance between every two segments is calculated simultaneously. According to the superposition theory of electromagnetic field, the total inductance can be calculated by accumulating the contribution of each line segment. In order to eliminate the influence of magnetic core on the calculation of self-inductance and mutual inductance, the multiple image method is adopted. It is also analyzed when there exists a misalignment. Meanwhile, the condition that the size of the coil on the primary side and secondary side are different is also considered.
2) A mathematical model for calculating the ac resistance of the DD coil with ferrite core is proposed. Biot–Savart law is adopted to calculate the magnetic distribution. The image method is applied to remove the effect of the core on the magnetic distribution. Due to the complex structure of rectangular DD coil, it is difficult to directly give the field strength distribution at any position on the coil cross section. Therefore, DD coil is divided into unit segments firstly. Then, the resistance of unit segments is solved, respectively. Finally, the total ac resistance of coil can be calculated by numerical integration, which is easy to program.
3) A genetic algorithm based on the proposed coil mathematical model is proposed to optimize the coil structure. Compared with the coil design based on FEA software, it can significantly save time. The computing time of the genetic algorithm based on the proposed coil mathematical model for optimizing the coil structure is only 48 s in this article.

The rest of this article is organized as follows. In Section II, the model for calculating self-inductance and mutual inductance of the coreless coil is introduced. In Section III, the theoretical model of rectangular DD coil with ferrite core for calculating the inductance and mutual inductance is proposed. In Section IV, the analytical model for calculating the ac resistance of the DD coil with ferrite core is built. In Section V, the simulation model and experiment system are built to verify the proposed model. And a genetic algorithm based on the proposed coil theoretical model is proposed to optimize the coil structure.

II. Modeling for Self-Inductance and Mutual Inductance of the Coreless DD Planar Coil

A. Inductance and Mutual Inductance Calculation for the Parallel Straight Filaments

The rectangular DD coil can be divided into multiple straight segments. According to the superposition principle of electromagnetic field, the whole DD coil can be calculated by accumulating the contribution of each line segment. The operation frequency of the Litz coil used for WPT in EV application is usually 85 kHz. The displacement current is not considered when analyzing the field distribution. The spatial field distribution

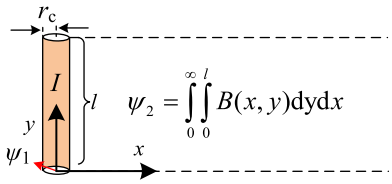

Fig. 3. Self-inductance of a straight wire.

is hardly affected by the current distribution in the conductor. When the coil is analyzed in the free space or air, the Biot–Savart law can be used to calculate the magnetic distribution. The self-inductance is decided by the amount of magnetic flux generated by the current in the conductor and linked with the conductor itself as shown in Fig. 3. The self-inductance of a straight round conductor can be gained by integrating the magnetic field in space.

Therefore, the self-inductance of a straight segment can be calculated by [44], [45]

$$L(l,r_c)=\frac{\psi_2+\psi_1}{I}=\frac{\mu_0}{2\pi}\left[l\cdot\mathrm{In}\left(\frac{l+\sqrt{l^2+r_c^2}}{r_c}\right)-\sqrt{l^2+r_c^2}+\frac{l}{4}+r_c\right] \tag{1}$$

where r_c is the radius of the round conductor and l is the length of the conductor, as shown in Fig. 3. Similarly, the mutual inductance of the parallel straight filaments can be obtained by [45]

$$\begin{aligned}M(l,m,d,\Delta)=&\frac{\mu_0}{4\pi}\left[\alpha\cdot\sinh^{-1}\left(\frac{\alpha}{d}\right)-\beta\cdot\sinh^{-1}\left(\frac{\beta}{d}\right)\right.\\&-\gamma\cdot\sinh^{-1}\left(\frac{\gamma}{d}\right)+\Delta\sinh^{-1}\left(\frac{\Delta}{d}\right)\\&\left.-\sqrt{\alpha^2+d^2}+\sqrt{\beta^2+d^2}+\sqrt{\gamma^2+d^2}-\sqrt{\Delta^2+d^2}\right]\\\alpha=l+m+\Delta,&\beta=l+\Delta,\gamma=m+\Delta\end{aligned} \tag{2}$$

where m and l are the lengths of the conductor, respectively. Δ is defined, as shown in Fig. 4(a). d is the distance between the two parallel conductors.

B. Mutual Calculation Principle for the Nonparallel Straight Filaments

The mutual inductance between two line segments at arbitrary positions, as shown in the Fig. 4(b), can be calculated according to the following equation [45]:

$$\begin{aligned}M(m,l,R_1,R_2,R_3,R_4)=&\frac{\mu_0}{4\pi}\cos(e)\left[2(u+l)\tanh^{-1}\left(\frac{m}{R_1+R_2}\right)\right.\\&-u\tanh^{-1}\left(\frac{m}{R_3+R_4}\right)+(v+m)\tanh^{-1}\left(\frac{l}{R_1+R_4}\right)\\&\left.-v\tanh^{-1}\left(\frac{l}{R_2+R_3}\right)\right]-\frac{\Omega d}{\sin(e)}\end{aligned} \tag{3}$$

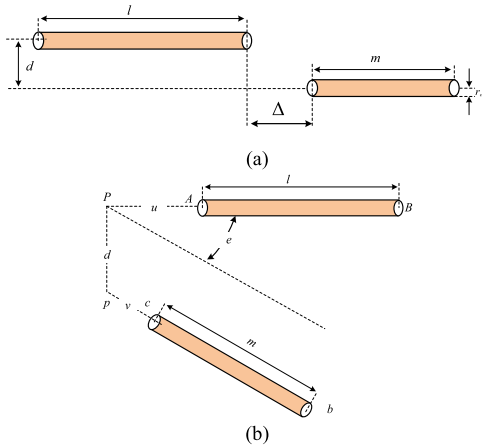

Fig. 4. (a) Parallel misaligned conductor. (b) Any position conductor.

where

$$\begin{aligned}\Omega=&\tan^{-1}\left[\frac{d^2\cos(e)+(\mu+l)(v+m)\sin^2(e)}{dR_1\sin(e)}\right]\\&-\tan^{-1}\left[\frac{d^2\cos(e)+(\mu+l)(v)\sin^2(e)}{dR_2\sin(e)}\right]\\&+\tan^{-1}\left[\frac{d^2\cos(e)+\mu v\sin^2(e)}{dR_3\sin(e)}\right]\\&-\tan^{-1}\left[\frac{d^2\cos(e)+\mu(v+m)\sin^2(e)}{dR_4\sin(e)}\right]\end{aligned} \tag{4}$$

$$\begin{aligned}\cos(e)=&\frac{\alpha^2}{2lm}\\R_1=Bb,&R_2=Ba,R_3=Aa,\text{and}R_4=Ab\\\alpha^2=&R_4^2-R_3^2+R_2^2-R_1^2\\d^2=&R_3^2-u^2-v^2+2uv\cos(e)\\u=&l\frac{2m^2(R_2^2-R_3^2-l^2)+\alpha^2(R_4^2-R_3^2-m^2)}{4l^2m^2-\alpha^4}\\v=&m\frac{2l^2(R_4^2-R_3^2-m^2)+\alpha^2(R_2^2-R_3^2-l^2)}{4l^2m^2-\alpha^4}\end{aligned} \tag{5}$$

where R_1, R_2, R_3, and R_4 are defined as the distance between points: B and b, B and a, A and a, and A and b.

C. Self-Inductance for Coreless Coil

The planar DD coils consist of two rectangular coils connected in series in the opposite direction, as shown in Fig. 5(b). The model parameters of planar DD coils are defined in Fig. 5. r_c is the radius of the round wire. W_{xp} and L_{yp} are the width and length of the primary DD coil. d_{sp} is the turn space defined as the distance between the center of the two adjacent wires. These parameters satisfy

$$W_{xp}=2W_{x1}+d_1, W_{x1}=2d_{sp}(N_1-1)+d_{w1}. \tag{6}$$

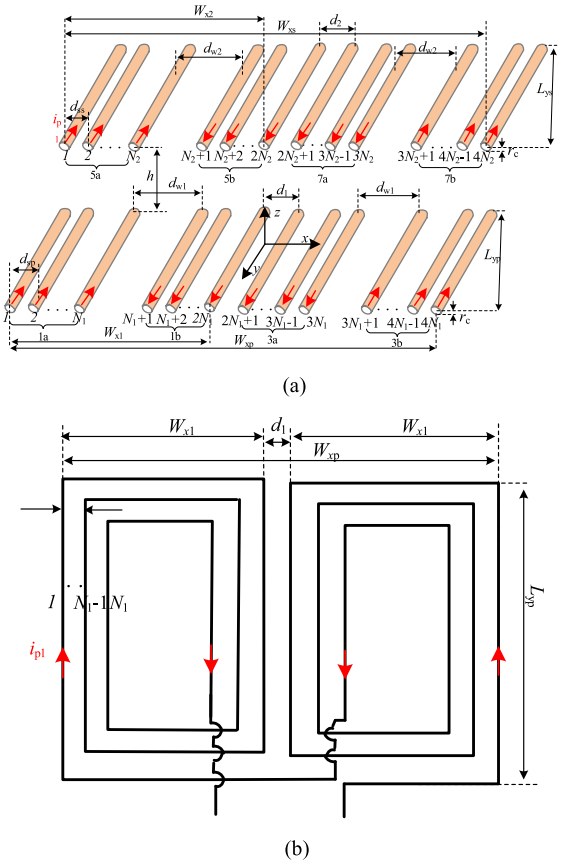

Fig. 5. Structure of the DD coil. (a) Cross-sectional view. (b) 2-D view.

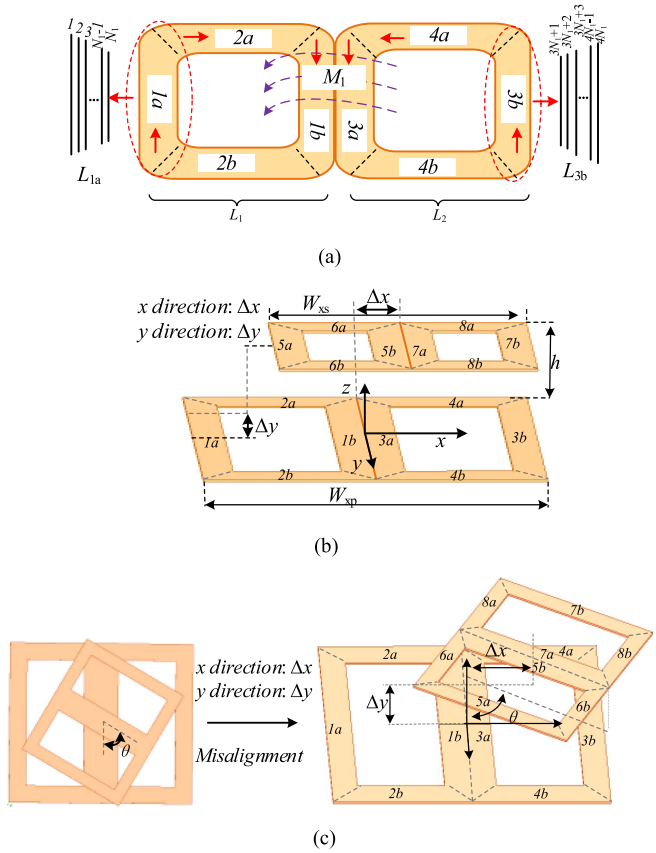

Fig. 6. Schematic diagram of planar DD coil. (a) Primary coil. (b) Coils on both sides with latera misalignment. (c) Coils on both sides with angular misalignment.

The inductance of the plane DD coil can be gained by

$$L = L_1 + L_2 + 2M_1 \tag{7}$$

where L_1 and L_2 are the self-inductance of the rectangular coils connected in series. M_1 is the mutual inductance between the two rectangular coils, as shown in Fig. 6(a).

The single rectangular coils L_1 and L_2 are separately divided into four parts: 1a, 1b, 2a, and 2b and 3a, 3b, 4a, and 4b. The value of M_1 can be gained by

$$M_1 = M_{1a3a} + M_{1a3b} + M_{1b3a} + M_{1b3b} \tag{8}$$

where M_{1a3a} is the mutual inductance between parts 1a and 3a in Fig. 6(a). M_{1a3a} can be calculated by

$$|M_{1a3a}| = \sum_{i=2N_1+1}^{3N_1} \sum_{j=1}^{N_1} M(\bar{l}_{1a}, \bar{l}_{3a}, d_{ij\_1a3a}, \Delta_{1a3a})$$

$$\bar{l}_{1a} = \bar{l}_{3a} = L_{yp} - d_{sp}(N_1 - 1), d_{ij\_1a3a} = (i - j - 2)\, d_{sp} + d_{w1} + d_1$$

$$\Delta_{1a3a} = -(L_{yp} - d_{sp}(N_1 - 1)). \tag{9}$$

According to (2) and (9), the mutual inductance M_{1a3a} can be calculated. The $\bar{l}_{1a}$ and $\bar{l}_{3a}$ are defined as the average length of parts 1a and 3a. The definition of M_{1a3b}, M_{1b3a}, and M_{1b3b} is similar to M_{1a3a}.M_{1a3b}, M_{1b3a}, and M_{1b3b} can be calculated by

$$|M_{1a3b}| = \sum_{i=3N_1+1}^{4N_1} \sum_{j=1}^{N_1} M(\bar{l}_{1a}, \bar{l}_{3b}, d_{ij\_1a3b}, \Delta_{1a3b})$$

$$|M_{1b3a}| = \sum_{i=2N_1+1}^{3N_1} \sum_{j=N_1+1}^{2N_1} M(\bar{l}_{1b}, \bar{l}_{3a}, d_{ij\_1b3a}, \Delta_{1b3a})$$

$$|M_{1b3b}| = \sum_{i=3N_1+1}^{4N_1} \sum_{j=N_1+1}^{2N_1} M\left(\bar{l}_{1b}, \bar{l}_{3b}, d_{ij\_1b3b}, \Delta_{1b3b}\right)$$

$$\bar{l}_{1a} = \bar{l}_{3a} = \bar{l}_{3b} = \bar{l}_{1b} = L_{yp} - d_{sp}(N_1 - 1)$$

$$\Delta_{1a3b} = \Delta_{1b3a} = \Delta_{1b3b} = -\left(L_{yp} - d_{sp}(N_1 - 1)\right)$$

$$d_{ij\_1a3b} = (i - j - 3)d_{sp} + 2d_{w1} + d_1, d_{ij\_1b3a}$$

$$= (i - j - 1)\, d_{sp} + d_1$$

$$d_{ij\_1b3b} = (i - j - 2)d_{sp} + d_{w1} + d_1. \tag{10}$$

It should be noted that the value of the mutual inductance may be negative or positive. It is decided by the direction of the current in each part, as shown in Fig. 6. For example, the current in the part 1a and part 3a are opposite. and the value of M_{1a3a} is negative. When the two rectangular coils have the same turns

and size, there is $M_{1a3a} = M_{1b3b}$. L_1 can be obtained by

$$L_1 = L_{1a} + L_{1b} + L_{2a} + L_{2b} + 2M_{1a1b} + 2M_{2a2b} \quad (11)$$

where M_{1a1b} and M_{2a2b} are the mutual inductance between parts 1a and 1b and parts 2a and 2b. L_{1a}, L_{1b}, L_{2a}, and L_{2b} are the self-inductance of each part. M_{1a1b} and M_{2a2b} can be calculated by

$$\begin{aligned}
|M_{1a1b}| &= \sum_{i=1}^{N_1}\sum_{j=1}^{N_1} M(\bar{l}_{1a}, \bar{l}_{1b}, d_{ij_1a1b}, \Delta_{1a1b}) \\
|M_{2a2b}| &= \sum_{i=1}^{N_1}\sum_{j=i}^{N_1} M(\bar{l}_{2a}, \bar{l}_{2b}, d_{ij_2a2b}, \Delta_{2a2b}) \\
\bar{l}_{1b} &= \bar{l}_{1a} = L_{yp} - d_{sp}(N_1 - 1) \\
\bar{l}_{2b} &= \bar{l}_{2a} = W_{xp} - d_{sp}(N_1 - 1) \\
d_{ij_2a2b} &= (i-j-1)d_{sp} + L_{yp} - 2(N_1 - 1)d_{sp} \\
d_{ij_1a1b} &= (i-j-1)d_{sp} + d_{w1} \\
\Delta_{1a1b} &= L_{yp} - d_{sp}(N_1 - 1) \\
\Delta_{2a2b} &= W_{xp} - d_{sp}(N_1 - 1).
\end{aligned} \quad (12)$$

L_{1a} and L_{1b} have the same number of lines and are of the same length. Therefore, L_{1a} and L_{1b} have the same value. L_{1a} can be gained by

$$\begin{aligned}
L_{1a} &= \sum_{i=1}^{i=N_1} L(r_c, l_{i_1a}) + \sum_{i=1}^{i=N_1}\sum_{j=1,j\neq i}^{j=N_1} \\
&\quad \times M(\bar{l}_{1a}, \bar{l}_{1a}, d_{ij_1a}, -\bar{l}_{1a}/2) \\
\bar{l}_{1a} &= L_{yp} - d_{sp}(N_1 - 1), l_{i_1a} = L_{yp} - 2d_{sp}(i-1) \\
d_{ij_1a} &= (|i-j|)d_{sp}.
\end{aligned} \quad (13)$$

L_{2b} and L_{2a} have the same value. L_{2a} can be calculated by

$$\begin{aligned}
L_{2a} &= \sum_{i=1}^{i=N} L(r_c, l_{i_2a}) + \sum_{i=1}^{i=N}\sum_{j=1,j\neq i}^{j=N} \\
&\quad \times M(\bar{l}_{2a}, \bar{l}_{2a}, d_{ij_2a}, -\bar{l}_{2a}/2) \\
\bar{l}_{2a} &= W_{xp} - d_{sp}(N_1 - 1), l_{i_2a} = W_{xp} - 2d_{sp}(i-1) \\
d_{ij_2a} &= (|i-j|)d_{sp}.
\end{aligned} \quad (14)$$

L_2 can be calculated in the same way as L_1. If the two rectangular coils have the same turns and size, L_1 is equal to L_2. Due to space limitations, only the case that the two rectangular are identical is analyzed. The self-inductance of the coreless DD planar coils $L_{coreless}$ can be gained by

$$\begin{aligned}
L_{coreless} = 2\Bigg(& 2\sum_{i=1}^{i=N_1}(L(r_c, l_{i_1a}) + L(r_c, l_{i_2a})) \\
&+2\sum_{i=1}^{i=N_1}\sum_{j=1,j\neq i}^{j=N_1}(M(\bar{l}_{2a}, \bar{l}_{2a}, d_{ij_2a}, -\bar{l}_{2a}) \\
&+M(\bar{l}_{1a}, \bar{l}_{1a}, d_{ij_1a}, -\bar{l}_{1a})) \\
&+2\Bigg(\sum_{i=1}^{N_1}\sum_{j=1}^{N_1} M(\bar{l}_{1a}, \bar{l}_{1b}, d_{ij_1a1b}, \Delta_{1a1b}) \\
&+\sum_{i=1}^{N_1}\sum_{j=i}^{N_1} M(\bar{l}_{2a}, \bar{l}_{2b}, d_{ij_2a2b}, \Delta_{2a2b})\Bigg)\Bigg) \\
&+2\Bigg(\sum_{i=1}^{N_1}\sum_{j=i}^{N_1}(M(\bar{l}_{1a}, \bar{l}_{3a}, d_{ij_1a3a}, \Delta_{1a3a}) \\
&+M(\bar{l}_{1b}, \bar{l}_{3b}, d_{ij_1b3b}, \Delta_{1b3b}) \\
&+2\Bigg(\sum_{i=1}^{N_1}\sum_{j=1}^{N_1}(M(\bar{l}_{3b}, \bar{l}_{1a}, d_{ij_1a3b}, \Delta_{1a3b}) \\
&+M(\bar{l}_{3a}, \bar{l}_{1b}, d_{ij_1b3a}, \Delta_{1b3a})\Bigg).
\end{aligned} \quad (15)$$

C. Mutual Inductance Calculation Principle for Coreless DD Coil

The two coupled planar DD coils are divided into eight parts, as shown in Fig. 6(b). The mutual inductance between the coreless DD planar coil on the primary side and secondary side. $M_{coreless}$ can be calculated by

$$\begin{aligned}
M_{coreless} = \sum_{i=1}^{2}\sum_{j=0}^{3}\big(& M_{(2i-1)a(j+5)b} + M_{(2i-1)a(j+5)a} + M_{(2i-1)b(j+5)b} \\
&+ M_{(2i-1)b(j+5)a} + M_{(2i)a(j+5)b} + M_{(2i)a(j+5)a} \\
&+ M_{(}2i)b(j+5)b + M_{(2i)b(j+5)a}\big).
\end{aligned} \quad (16)$$

When there exists lateral misalignment, only M_{1a7a} is taken as an example due to the limitation of space, which can be calculated by

$$\begin{aligned}
|M_{1a7a}| &= \sum_{i=1}^{N_2}\sum_{j=i}^{N_1} M(\bar{l}_{1a}, \bar{l}_{7a}, d_{ij_1a7a}, \Delta_{1a7a}) \\
\bar{l}_{1a} &= L_{yp} - d_{sp}(N_1 - 1), \bar{l}_{7a} = L_{ys} - d_{sp(N_2-1)} \\
d_{ij_1a7a_x} &= (jd_{ss} - id_{sp}) + W_{x1} + (d_2 + d_1)/2 + \Delta x \\
d_{ij_1a7a} &= (d_{ij_1a7a_x})^2 + h^2, \Delta_{1a7a} = -(L_{yp} + L_{ys})/2 + \Delta y
\end{aligned} \quad (17)$$

where Δx and Δy are the misalignment distance in the x- and y-directions, as shown in Fig. 6(b). The other parameters in (17) are shown in Fig. 5. The calculation process is similar for mutual inductance. Therefore, combining (1), (2), (16), and (17), the mutual inductance between the coil on the primary side and secondary side can be calculated with the arbitrary position.

When there exists lateral misalignment and angular misalignment, M_{1a7a} is taken as an example due to the limitation of space. The rotation angle is defined as in the Fig. 6(c). The relative position of the two coils can be seen as that the secondary coil rotates around the coil center point and then horizontally

misalign, as shown in the Fig. 6(c).

$$|M_{1a7a}| = \sum_{i=1}^{N_2}\sum_{j=i}^{N_1} M\left(\bar{l}_{1a}, \bar{l}_{7a}, \times R_{1_{1a7a\_ij}}, R_{2_{1a7a\_ij}}, R_{3_{1a7a\_ij}}, R_{4_{1a7a\_ij}}\right)$$
$$\bar{l}_{1a} = L_{yp} - d_{sp}(N_1 - 1), \bar{l}_{7a} = L_{ys} - d_{sp}(N_2 - 1) \quad (18)$$

where the R_{11a7a_ij} is defined as the distance between point B of the *i*th straight segment in part 7a of the secondary coil and Point b of the *j*th straight segment in part 1a of the primary coil. The R_{21a7a_ij} is defined as the distance between point B of the *i*th straight segment in part 7a of the secondary coil and Point a of the *j*th straight segment in part 1a of the primary coil. The R_{31a7a_ij} is defined as the distance between point A of the *i*th straight segment in part 7a of the secondary coil and Point a of the *j*th straight segment in part 1a of the primary coil. The R_{41a7a_ij} is defined as the distance between point A of the *i*th straight segment in part 7a of the secondary coil and Point b of the *j*th straight segment in part 1a of the primary coil. R_{11a7a_ij}, R_{21a7a_ij}, R_{31a7a_ij}, R_{41a7a_ij} can be gained according the misalignment distance Δx, Δy, and angular angle θ.

III. Modeling for Self-Inductance and Mutual Inductance Calculation of Planar DD Coil With Ferrite Core Shielding

For eliminating the leakage flux and improving the coupling between the coils, the ferrite core is usually adopted for optimizing the flux distribution. Due to the ferrite core, magnetic field distribution becomes difficult to calculate directly.

Fortunately, the image method can be adopted for DD planar coil covered with ferrite. In the DD coil, as shown in Fig. 6(a), the current direction in parts 1b and 3a is opposite to that in parts 1a and 3b. Therefore, in the area outside the DD coil, the magnetic flux generated by currents in 1b, 3a and 1a, 3b cancels each other. The magnetic field generated by the DD coil decays very fast outside the DD coil area, and the magnetic field is mainly concentrated inside the DD coil area, as shown in Fig. 7. The 3-D simulation results of the magnetic distribution are gained by the Maxwell software. Fig. 7(c) shows the magnetic distribution of the rectangular coil with the same self-inductance value, turn clearances, and size as the DD coil. The legend in the figure adopts logarithmic coordinates to better display the magnetic field distribution outside the coil area. It can be seen that the magnetic field distribution of the DD coil is more obviously concentrated compared with a single rectangular coil. When the DD coil is covered with the same size ferrite core, the field distribution generated by the coil is approximately the same as when the DD coil is placed on the magnetic core whose size is much larger than the area of the coil. Although there is still a small part of magnetic flux outside the coil area, it has a very limited contribution to coil self-inductance and mutual inductance. Therefore, the mirror method can be used when the DD coil is covered with a magnetic core.

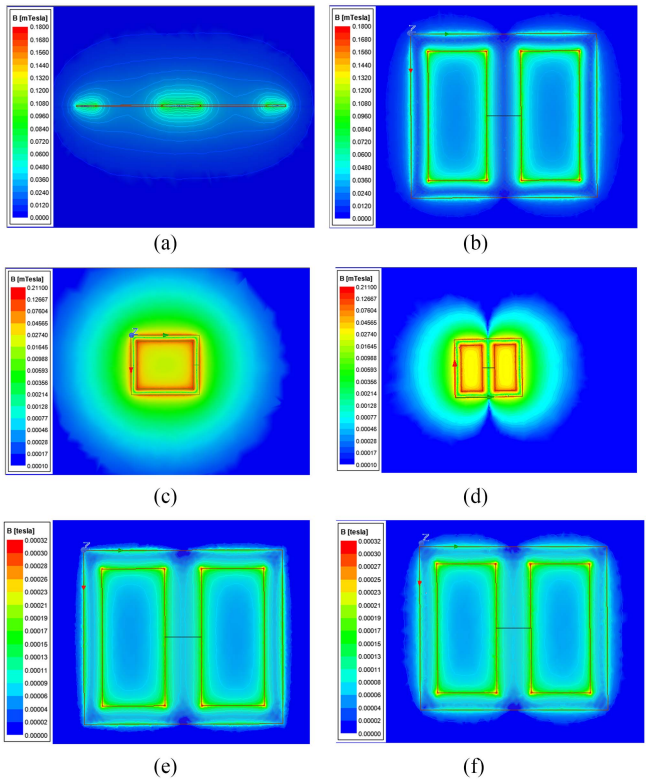

Fig. 7. (a) Magnetic distribution on the *xz*-plane, coreless DD coil. (b) Magnetic distribution on the *xy*-plane, coreless DD coil. (c) Magnetic distribution on the *xy*-plane (logarithm used in legend), rectangular coreless coil. (d) Magnetic distribution on the *xy*-plane (logarithm used in legend), DD coreless coil. (e) Magnetic distribution on the *xy*-plane, DD coil with the same size ferrite core. (f) Magnetic distribution on the *xy*-plane, DD coil with ferrite core 16 times larger than the size of the coil.

When the thickness of the core is finite, the multiple mirroring method can be used [46]. Actually when the relative permeability of the ferrite core is usually very large, the thickness of the ferrite core has little impact on the inductance and mutual inductance. Therefore, mirroring once is enough for calculating the self-inductance and mutual inductance due to the ferrite core on the same side. However, the ferrite core on the secondary side also affects the self-inductance of the coil on the primary side. Considering the effect of the core on the other side, the multiple mirroring method can be used. The conductor can be regarded as being placed between two parallel magnetic cores, as shown in Fig. 8(a). Theoretically, the conductors between the parallel magnetic plates need to be mirrored countless times [47]. For the *n*th time of mirroring image current satisfies

$$I_{\mathrm{p2n-2}} = I_{\mathrm{p}}\left(\frac{u_{\mathrm{r}}-1}{u_{\mathrm{r}}+1}\right)^{\mathrm{n-1}}, I_{\mathrm{p2n-1}} = I_{\mathrm{p}}\left(\frac{u_{\mathrm{r}}-1}{u_{\mathrm{r}}+1}\right)^{\mathrm{n}}. \quad (19)$$

When it is the *n*th time of mirroring, the distance between image coil $L_{2n\text{-}2}$, $L_{2n\text{-}1}$ and original coil L_{p} satisfies

$$h_{\mathrm{p1p2n-2}} = 2h_{fe}\cdot floor(\mathrm{n}/2) + 2d_{fe}(n-2)$$
$$h_{\mathrm{p1p2n-1}} = 2h_{fe}\cdot floor(\mathrm{n}/2) + 2d_{fe}(n-1) \quad (20)$$

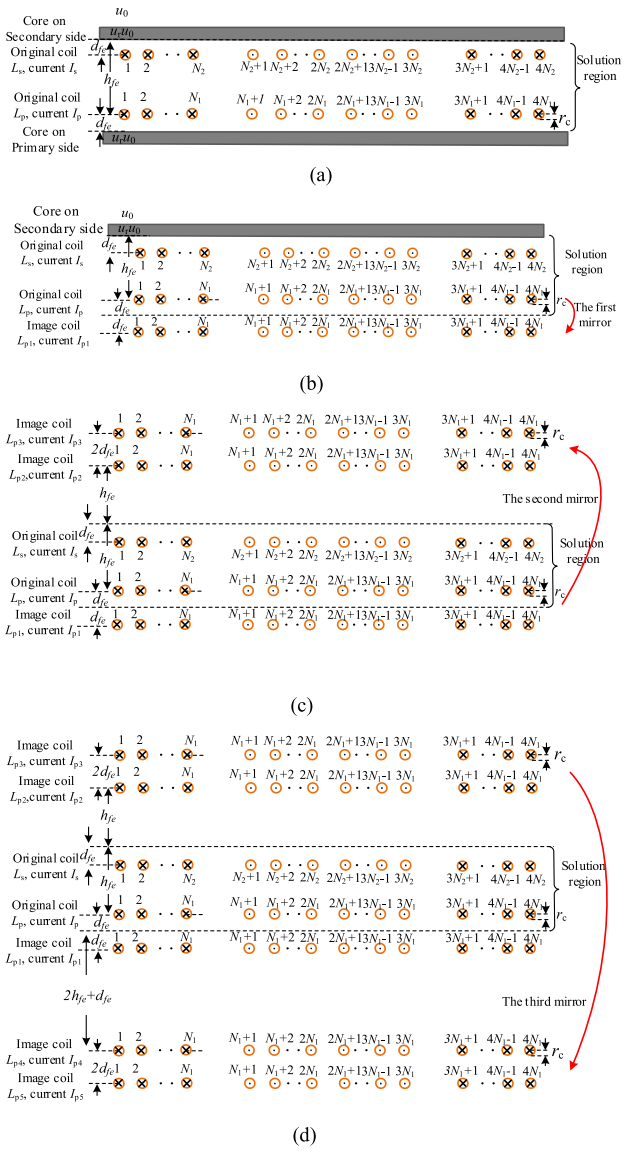

Fig. 8. (a) Cross section of DD coil. (b) First time of mirroring. (c) Second time of mirroring. (d) Third time of mirroring.

where the floor(n/2) means the maximum integer that does not exceed n/2. Theoretically, the conductors between the parallel magnetic plates need to be mirrored countless times. Usually, an accurate result can be obtained by mirroring twice for calculating the self-inductance except that the magnetic core on the secondary side is very close to the coil on the primary side. Therefore, the self-inductance L_{p} can be calculated by

$$L_{\mathrm{p}} = L_{\mathrm{p\_coreless}} + M_{\mathrm{LpLp1}} + M_{\mathrm{LpLp2}} + M_{\mathrm{LpLp3}}. \tag{21}$$

$L_{\mathrm{p\_coreless}}$ is the self-inductance of the coil without ferrite, which can be calculated by the method mentioned in the previous section. M_{LpLp1}, M_{LpLp2}, and M_{LpLp3} are the mutual inductance between the original coil and the image coil, which can be also calculated by the method mentioned in the previous section. The mutual inductance between the coils with ferrite can be gained by

$$M_{\mathrm{DD}} = \sum_{\mathrm{i}=1}^{n} \left(\frac{I_{\mathrm{p}2i\text{-}2}}{I_{\mathrm{p}}} M_{\mathrm{LsLp}2i-2} + \frac{I_{\mathrm{p}2i\text{-}2}}{I_{\mathrm{p}}} M_{\mathrm{LsLp}2i-1} \right) \tag{22}$$

where the n is the coil mirror time. The $M_{\mathrm{LsLp2n\text{-}1}}$, $M_{\mathrm{LsLp2n\text{-}2}}$ are the mutual inductance between the coil L_{s} and the image coil $L_{\mathrm{P2i\text{-}1}}$, $L_{\mathrm{P2i\text{-}2}}$ separately, which can be calculated by the method mentioned in the previous section. Similarly, it needs to mirror countless times for obtaining the value of mutual inductance between the DD coil with ferrite. Actually, a relatively accurate result can be obtained by several times mirroring. When the air gap is small, it needs more times of mirroring. The eddy current in the ferrite core is so small that has little contribution to the magnetic distribution in the air. Therefore, the eddy current is not considered. The self-inductance and mutual inductance can be calculated based on the multiple mirror method and the Biot–Savart law.

IV. Modeling for AC Resistance of Planar DD Coil With Ferrite Shielding

A. AC Resistance of Litz Wire

The Litz wire is composed of a number of strands that are usually wrapped in insulating paint. In an ideal Litz wire, all the strands circulate between all possible positions in the bundle, and all are the same length. Each strand in the wire has the same impedance. Therefore, it is considered that each strand has the same current [42]. The power dissipation per unit length of the conductor is defined by

$$R = \frac{\int_A \int_0^T \mathrm{J}(x,y,t)^2 dt dA}{I^2}. \tag{23}$$

The ac resistance of each strand is decided by the current distribution. The current distribution of a conductor is affected by the skin effect and proximity effect. Since the electromagnetic field satisfies the superposition theorem, the current caused by the skin effect and proximity can be calculated separately. In [48], it has been proved that the loss caused by skin effect and proximity is orthogonal. The ac resistance can be gained by

$$\begin{aligned} P_{\mathrm{total}} &= P_{\mathrm{skin}} + P_{\mathrm{appr}} \\ R_{\mathrm{total}} &= R_{\mathrm{skin}} + R_{\mathrm{appr}} = P_{\mathrm{total}} / I^2. \end{aligned} \tag{24}$$

The R_{skin} and R_{pro} are the resistances caused by the skin effect and proximity respectively. The I is the current through the conductor. The R_{skin} per unit of length can be calculated by (21) [48]

$$\begin{aligned} R_{\mathrm{skin\_u1}} &= \frac{\sqrt{\mu\sigma\omega}}{2\pi n_0 r_0 \sigma} \frac{\left(ber_0(\xi)\, bei'(\xi) - ber'(\xi)\, bei_0(\xi)\right)}{\left(ber'(\xi)\right)^2 + \left(bei'(\xi)\right)^2} \\ ber' &= \left(ber_1 + bei_1\right)/\sqrt{2} \\ bei' &= \left(-ber_1 + bei_1\right)/\sqrt{2} \\ \xi &= r_0\sqrt{\mu\sigma\omega} \end{aligned} \tag{25}$$

where the r_0 is the ratio of the strand and n_0 is the number of the strand. σ is the conductivity of the conductor and the μ the

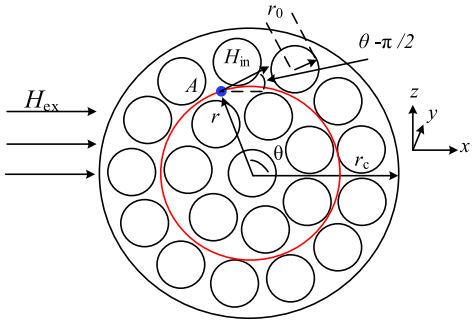

Fig. 9. Magnetic on the cross section of the Litz wire.

permeability. ω is operation angular frequency. ber_0, bei_0, ber_1, and bei_1 are the kelvin function. Actually, the value of R_{skin} is approximately equal to the dc resistance of the Litz wire when the ratio of the strand is small enough. The R_{appr} per unit of length can be calculated by (20) [48]

$$R_{\text{appr\_u1}} = -\frac{2\pi\xi n_0}{\sigma}\frac{ber_2(\xi)\,ber'(\xi)+bei_2(\xi)\,bei'(\xi)}{ber_0(\xi)^2+bei_0(\xi)^2}H^2 \tag{26}$$

ber_2 and bei_2 are the kelvin function. H is the magnetic field strength of the conductor cross section. It can be seen that the key to calculating the R_{appr} is to obtain the magnetic distribution H. The length of the strand is increased by twisting, which will increase the dc resistance of the coil. The dc resistance is proportional to the length of the conductor. Therefore, the real length of the strand can be calculated by (23) [49]

$$l_{\text{strand}} = l_{\text{wire}} R_{\text{dc\_test}}/R_{\text{dc\_cal}} \tag{27}$$

where l_{wire} is the length of the Litz wire. $R_{\text{dc·test}}$ is the tested dc value and the $R_{\text{dc·cal}}$ is the theoretically calculated dc value. The ac resistance of the Litz wire can be rewritten as

$$R_{\text{total}} = (R_{\text{skin\_u1}}+R_{\text{appr\_u1}})\,l_{wire}\frac{R_{\text{dc\_test}}}{R_{\text{dc\_cal}}}. \tag{28}$$

B. Magnetic Distribution Analysis

The magnetic strength of the conductor cross section consists of two parts: H_{in} and H_{ex}, as shown in Fig. 9. H_{in} is generated by the current inside the Litz conductor. H_{ex} is generated by the current in other turns. H_{in} at the point A (x,y,z) in the Litz wire, as shown in Fig. 9, can be calculated by

$$\begin{aligned} 2\pi r\overrightarrow{H}_{\text{in}} &= \frac{\pi r^2 I}{\pi r_c^2} \\ 2\pi r H_{\text{in\_x}} &= 2\pi H_{\text{in}}\sin(\theta) \\ 2\pi r H_{\text{in\_z}} &= -2\pi r H_{\text{in}}\cos(\theta) \end{aligned} \tag{29}$$

where $H_{\text{in·x}}$ and $H_{\text{in·z}}$ are the components H_{in} on the x- and z-axes. The H_{ex} generated by the rest of the turns at point A (x,y,z) can be calculated based on the multiple mirror image and Biot–Savart law.

The magnetic strength at point A generated by a straight filament with length L, as shown in Fig. 10, can be calculated by (26) [38]

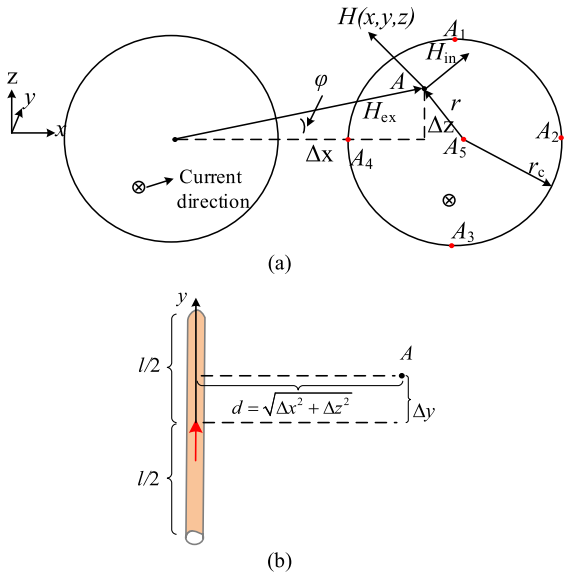

Fig. 10. (a) Cross section through point A and perpendicular to the y-axis. (b) Relative position between point A and the straight wire.

$$\begin{aligned} \overrightarrow{H}(\Delta x,\Delta y,\Delta z) &= \frac{1}{4\pi}\oint_l \frac{Idl\times e_R}{R^2} \\ &= \frac{I}{4\pi d}\left[\frac{\Delta y+l/2}{\sqrt{d^2+(\Delta y+l/2)}}-\frac{\Delta y-l/2}{\sqrt{d^2+(\Delta y-l/2)}}\right]e_\phi \\ H\_x &= H(\Delta x,\Delta y,\Delta z)\sin(\varphi) \\ &= H(\Delta x,\Delta y,\Delta z)\frac{\Delta z}{\sqrt{\Delta^2 x+\Delta^2 z}} \\ H\_z &= H(\Delta x,\Delta y,\Delta z)\frac{\Delta x}{\sqrt{\Delta^2 x+\Delta^2 z}} \end{aligned} \tag{30}$$

where Δx and Δz are defined as the distance between the two conductors on the x- and z-axes. The Δy is defined as the distance between point A and the midpoint of the conductor. The direction of e_ϕ is perpendicular to the plane formed by the straight wire and point A.

When it is a DD coil with a core, as shown in Fig. 11, the image method is used to remove the ferrite core. The original coil is divided into N_{X} segments along the wire direction, and the length of each segment is Δl, as shown in Fig. 11(b). The calculation of the magnetic strength H_{ex} at point A_1 in the N_1+1th conductor is taken as an example, as shown in Fig. 11(b). Point A_1 is located in the jth segment of the coil. The position of point A_1 on the cross section of the conductor is shown in Fig. 10(a). According to the superposition theorem of electromagnetic field, the H_{ex} at point A_1 can be calculated by

$$H_{\text{ex\_}jA1}=\sum_{i=1}^{4}(H_{\text{ia\_}j}+H_{\text{ib\_}j}+H_{\text{ia1\_}j}+H_{\text{ib1\_}j}) \tag{31}$$

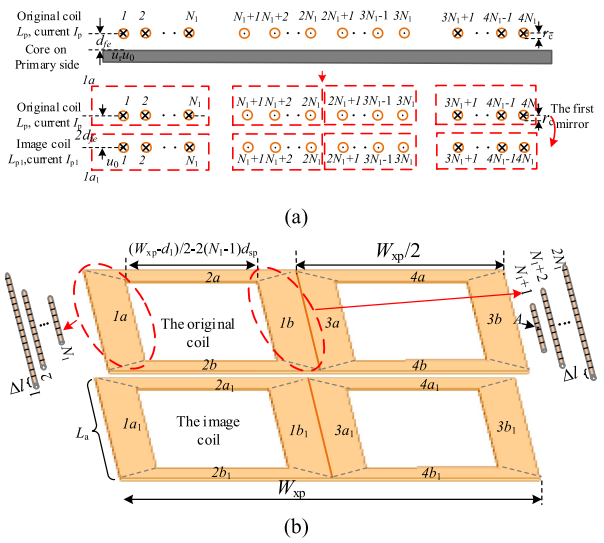

Fig. 11. (a) Cross section of the DD coil. (b) DD coil after mirroring.

where H_{ia_j} and H_{ib_j} are the magnetic strength generated by the *i*a and *i*b part of the original coil, as shown in Fig. 11. The H_{ia_j} and H_{ib_j} is the magnetic strength generated by the 1a and 1b parts of the image coil. The value of H_{ia_j}, H_{ib_j}, H_{ia1_j}, and H_{ib1_j} are calculated in (37)–(40) in Appendix. The magnetic strength at point A_1 generated by each part of the coil can be calculated by adding up the contribution of each conductor. The contribution of each conductor can be calculated by (30). It should be noted that point $\underline{A}_1$ is in the N_1+1th conductor that belongs to the 1b part of the coil. Therefore, H_{1b} does not contain the contribution of the N_1+1th conductor. The total magnetic strength at point *A* can be obtained by

$$\begin{aligned}\overrightarrow{H}_{j\_A1} &= \overrightarrow{H}_{ex\_jA1}+\overrightarrow{H}_{in}\\ H_{xj\_A1} &= H_{ex\_jA1}\frac{\Delta z}{\sqrt{\Delta^2 x+\Delta^2 z}}+2\pi r H_{in}\sin(\theta)\\ H_{zj\_A1} &= H_{ex\_jA1}\frac{\Delta x}{\sqrt{\Delta^2 x+\Delta^2 z}}-2\pi r H_{in}\cos(\theta).\end{aligned} \tag{32}$$

H_{xj} and H_{zj} are the components of total magnetic strength H_j on the *x*- and *z*-axes. *j* means the *j*th segment of the coil. The magnetic strength on the cross section of the conductor is not uniform. Therefore, five points on the section of the conductor are selected to calculate the average of the squared field for replacing the magnetic strength on the cross section of the conductor, as shown in the Fig. 10(a). The cross-sectional average squared field can be calculated by

$$H_j=\sqrt{\frac{\sum_{i=1}^{5}H_{jAi}^2}{5}}==\sqrt{\frac{\sum_{i=1}^{5}\left(H_{xjAi}^2+H_{zjAi}^2\right)}{5}} \tag{33}$$

where H_{jAi} means the magnetic strength at point A_i on the section of the *j*th segment conductor of the coil. When the value of Δl is small enough, the cross-sectional average squared field can be considered the same value. The resistance in the *j*th

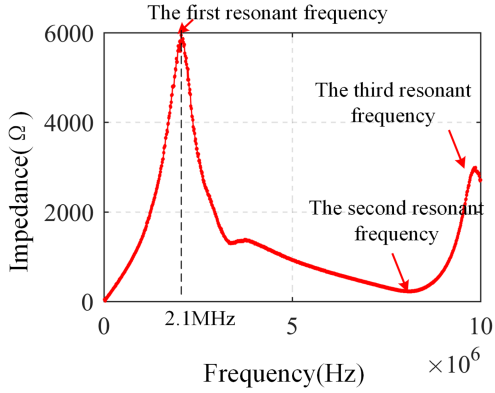

Fig. 12. Impedance amplitude frequency curve of the DD coil A.

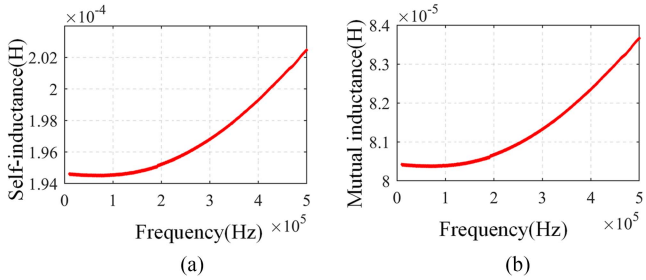

Fig. 13. Inductance against the frequency. (a) Self-inductance. (b) Mutual inductance.

segment caused by the proximity effect can be calculated by

$$R_{appr\_j}=-\frac{2\pi\xi n_0}{\sigma}\frac{ber_2(\xi)\,ber'(\xi)+bei_2(\xi)\,bei'(\xi)}{ber_0(\xi)^2+bei_0(\xi)^2}H_j^2\Delta l. \tag{34}$$

According to (25), (26), (28), and (34), the total resistance of the DD can be calculated by

$$\begin{aligned}R_{total}=&\left(-\frac{2\pi\xi n_0}{\sigma}\frac{ber_2(\xi)\,ber'(\xi)+bei_2(\xi)\,bei'(\xi)}{ber_0(\xi)^2+bei_0(\xi)^2}\sum_{j=1}^{N_x}H_j^2\Delta l\right.\\ &\left.+\frac{\sqrt{\mu\sigma\omega}}{2\pi n_0 r_0\sigma}\frac{\left(ber_0(\xi)\,bei'(\xi)-ber'(\xi)\,bei_0(\xi)\right)}{\left(ber'(\xi)\right)^2+\left(bei'(\xi)\right)^2}\right)l_{wire}\\ &\times\frac{R_{dc\_test}}{R_{dc\_cal}}.\end{aligned} \tag{35}$$

V. Simulation and Experiment Verification

The WPT system for EV or the qi device usually operates far away from the self-resonant frequency especially for the EV WPT system. The operate frequency is usually within 200 kHz. Therefore, the displacement current is not considered and the effect caused by the parasitic capacitance can be ignored in this case. For verifying this assumption, the impedance and inductance of the coil are swept first, as shown in Figs. 12 and 13. It can be seen that the self-resonant frequency is above MHz. Within 500 kHz, the frequency has little effect on the inductance of coil. Therefore, the operation frequency is far

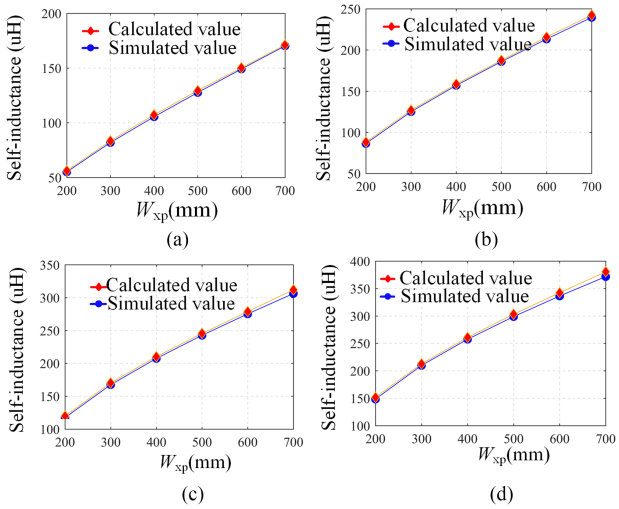

Fig. 14. Self-inductance with different W_{xp} when (a) L_{yp} is 200 mm, (b) L_{yp} is 300 mm, (c) L_{yp} is 400 mm, and (d) L_{yp} is 500 mm.

TABLE I
SIMULATION PARAMETERS IN FIG. 14

Symbol	Value	Symbol	Value	Symbol	Value
d_1	3 mm	r_c	1.5 mm	N_1	10
d_{sp}	3 mm				

from the self-resonant frequency and the parasitic capacitor can be ignored in this case.

A. Comparison Between the Simulation and the Theoretical Calculation Results

For verifying the accuracy of the proposed model, the 3-D FEA simulation is built. Fig. 14 shows the self-inductance of DD coils of different sizes. The distance between the coil and the ferrite core is 5 mm. The ferrite core and the coil have the same size. The thickness of the core is 5 mm. The other parameters of the DD coil are listed in Table I. It can be seen that the theoretical calculation values are in good agreement with the simulation results. The maximum error is within 5%.

The simulation results and calculated values of the mutual inductance between the DD coil with ferrite core on the primary side and secondary side are compared, as shown in Figs. 15 and 16. Fig. 15(a) shows the mutual inductance of the DD coupler with different coil sizes and, Fig. 15(b) shows the mutual inductance of the DD coupler with different distances between the coils. In Fig. 15, the size of the DD coils on the two sides is the same. The distance between the coils on the primary side and secondary side is 200 mm in Fig. 15(a). In Fig. 14, the size of DD coils on two sides is different. The thickness of the ferrite core is 5 mm. The other parameters unmentioned of the DD coils in Fig. 16 are listed in Table II. The theoretical calculation values are highly consistent with the simulation results. The maximum error is within 5%.

The calculated value of mutual inductance of the coupler is also compared with the simulated values, as shown in Figs. 17

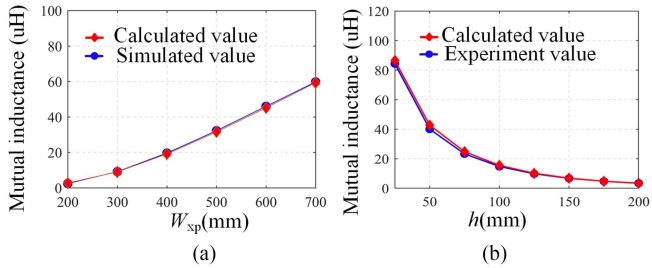

Fig. 15 (a) Mutual inductance with different coil sizes, $L_{yp} = L_{ys} = 400$ mm $N_1 = N_2 = 10$, and $d_{sp} = 3$ mm. (b) Mutual inductance with different air gap between the two sides $L_{yp} = L_{ys} = 200$ mm, $W_{xp} = W_{xs} = 400$ mm, $N_1 = N_2 = 7$, and $d_{sp} = 3$ mm.

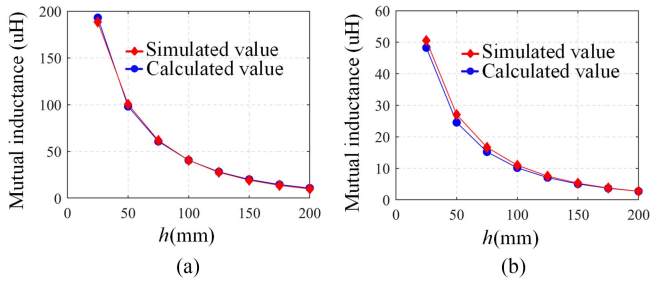

Fig. 16. Mutual inductance with different air gap between two sides when the coil on the two sides has a different size. (a) Turn number $N_1 = N_2 = 10$ and $d_{sp} = d_{ss} = 3.7$ mm. (b) Turn number $N_1 = N_2 = 5$ and $d_{sp} = d_{ss} = 7.4$ mm.

TABLE II
SIMULATION PARAMETERS IN FIG. 16

Symbol	Value	Symbol	Value	Symbol	Value
d_1	3.7 mm	r_c	1.8 mm	d_{fe}	1.7 mm
d_2	7.4 mm	W_{x1}	200 mm	L_{ys}	200 mm
W_{x2}	200 mm	L_{yp}	350 mm		

and 18 when misalignment exists. In Fig. 17, the coils on two sides have the same size. The distance d_{fe} is set at 1.7 mm. Fig. 17(a) and (b) shows the mutual inductance of the coupler against the misalignment distance in the x-axis, whereas Fig. 17(c), and (d) shows the mutual inductance against the misalignment distance in the y-axis. In Fig. 18, the coils on two sides have different sizes, of which the parameters are listed in Table II. The distance h between the coils on the primary side and secondary side is 100 mm in Fig. 18. Although there are errors in the process of misalignment, the variation trend of mutual inductance gained by calculation is consistent with the simulated value when there is misalignment.

For verifying the effectiveness of the proposed model when there exists angular misalignment, the calculation results are compared with the simulations and experiment results, as shown in the Fig. 19. The coils used for comparison have the same structure parameters as coil A. The distance between the coil is set 100 mm with $\Delta x = \Delta y = 0$. It can be seen that the theoretical calculation, simulation, and experimental results are in good agreement.

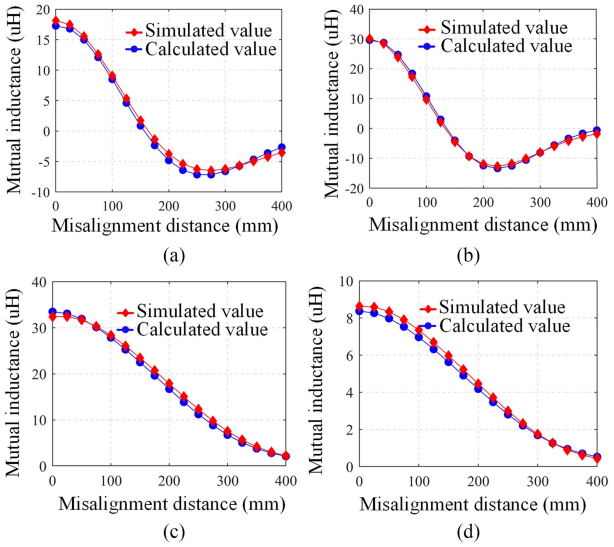

Fig. 17. Mutual inductance of the coupler with $L_{yp} = L_{ys} = 350$ mm and $W_{xp} = W_{xs} = 400$ mm. (a) $h = 200$ mm, $d_{sp} = d_{ss} = 3.7$ mm, $N_1 = N_2 = 10$, and misalignment in the x-axis. (b) $h = 160$ mm, $d_{sp} = d_{ss} = 3.7$ mm, $N_1 = N_2 = 10$, and misalignment on the x-axis. (c) $h = 150$ mm, $d_{sp} = d_{ss} = 3.7$ mm, $N_1 = N_2 = 10$, and misalignment on the y-axis. (d) $h = 150$ mm, $N_1 = N_2 = 5$, $d_{sp} = d_{ss} = 7.4$ mm, and misalignment on the y-axis.

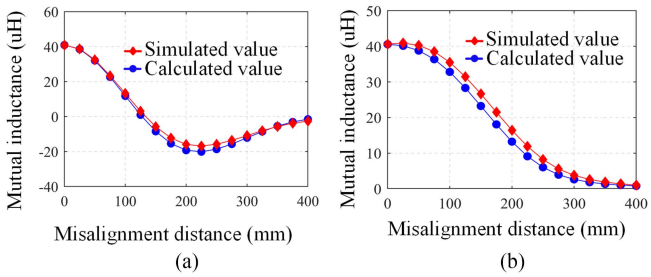

Fig. 18. Mutual inductance of coupler (a) $h = 100$ mm, $d_{sp} = d_{ss} = 3.7$ mm, $N_1 = N_2 = 10$, and misalignment on the x-axis. (b) $h = 100$ mm, $d_{sp} = d_{ss} = 3.7$ mm, $N_1 = N_2 = 10$, and misalignment on the y-axis.

TABLE III
TIME COMPARISON OF PROPOSED MODEL AND FEA SIMULATION

	Time of calculation	Time of simulation
Self-inductance	0.09 s	109 s
Mutual	0.59 s	109 s
AC resistance	6.5 s	1342 s (3-D model with ideal litz model in Maxwell)

In real applications, the coils may have chamfer corners of the rectangle. In this case, for verifying the effectiveness of the proposed method, the comparison between coil with chamfer corner and right angle corner is conducted, as shown in the Figs. 20 and 22. The coil models for comparison are depicted as the Fig. 21. Coil in Fig. 21(b) has the same structure parameters as the coil A. The only difference between coils in Fig. 21(a) and (b) is the corner.

The comparison of the time cost of the model and simulation is summarized in Table III.

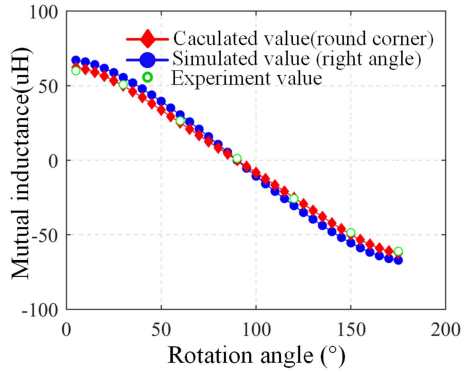

Fig. 19. Mutual inductance with different rotation angle.

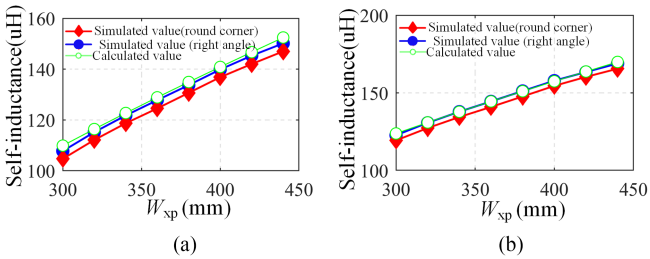

Fig. 20. Comparison of self-inductance between chamfered and non-chamfered coils with different coil size. (a) Coil length $L_{yp} = 260$ mm. (b) Coil length $L_{yp} = 290$ mm.

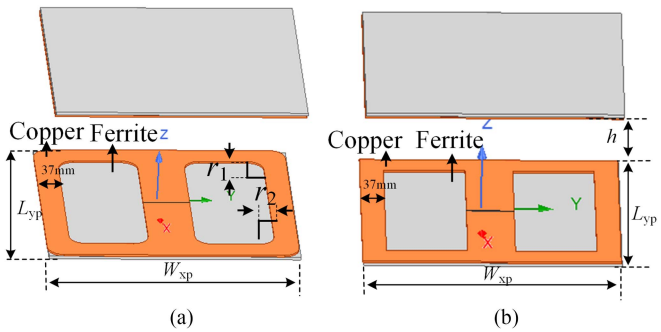

Fig. 21. Coil models for comparison. (a) Coil model with chamfer corner, $r_1 = r_2 = 20$ mm (b) Coil model with right angle corner.

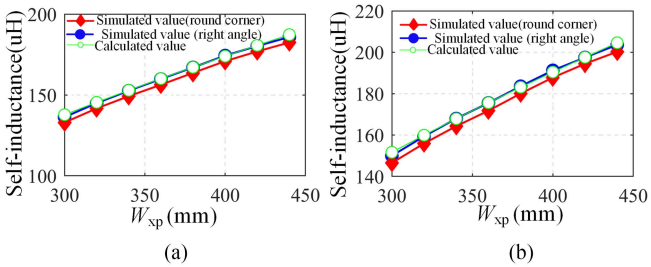

Fig. 22. Comparison of mutual inductance between chamfered and noncham-fered coils with different coil size, and the distance between the coils on primary side and secondary side is 100 mm. (a) Coil length $L_{yp} = 260$ mm. (b) Coil length $L_{yp} = 290$ mm.

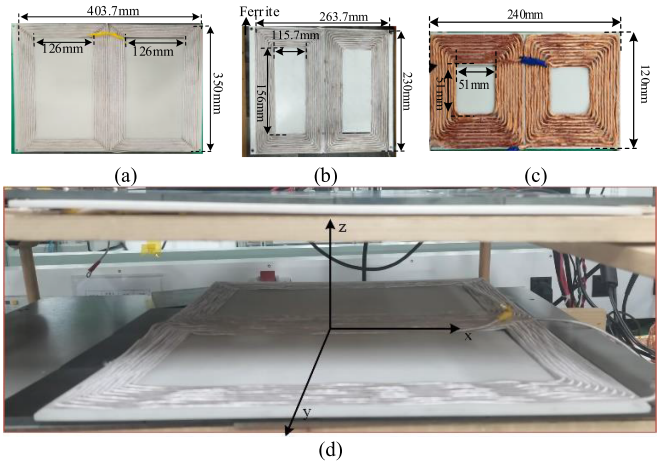

Fig. 23. Parts of the fabricated coils. (a) Coil A. (b) Coil D. (c) Coil C. (d) Coils on the primary side and secondary side have the same size of coil A.

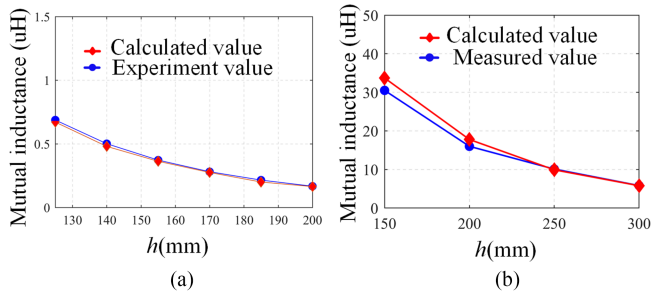

Fig. 24. Mutual inductance against the air gap between the coil. (a) Coils on the two sides has the same size as that of coil D. (b) Coils on the two sides have the same size as that of coil A.

Due to the difficulty of modeling the Litz wire coil directly, the simulation model of the coil adopts the ideal Litz model in Maxwell for comparison, which can reduce the difficulty and simulation time. The coil A is used for comparison. The value is calculated by MATLAB. The CPU is 3.6GHz and RAM is 16 GB.

B. Experiment Verification

For verifying the proposed model, some coils of different sizes are fabricated, as shown in Fig. 23. The theoretical calculation of mutual inductance between the coils in Fig. 23 is compared with experimental results, as shown in Fig. 24 with different air gaps. The parameters of the coil in Fig. 24 are listed in the Table V. Fig. 24(a) and (b) shows the mutual inductance with the different air gap between the coils. The coil in Fig. 24(a) is coreless and the coil in Fig. 24(b) is covered with ferrite. Fig. 25(a) shows the mutual inductance between the coils against the misalignment distance in the y-axis when the coils on the two sides have the same size. Fig. 25(b) shows the mutual inductance between the coils against the misalignment distance on the x-axis when the coils on the two sides have different sizes. When it is in alignment, the difference between the calculated value and the measured value is less than 6%. Although there exist relatively large errors at several points in the process of the misalignment, the error is within 15%. The variation trend of the calculated mutual inductance is still consistent with the measured values. The theoretical values of self-inductance with different coils structures are compared with the experimental values, as given in Table IV. The parameters of these coils are listed in Table V. The error is within 5%.

The ac resistance of these DD coils is measured by the LCR HIOKI IM3536. The theoretically calculated value is compared with the measured value, as shown in Fig. 26. The coil structure parameters are listed in Table V. The Litz wire type used is AWG-38. Within the frequency range 0–200 kHz, the error is less than 10%. It should be noted the error will increase as the frequency increase when the coil inductance is very large. There are three possible reasons causing the errors, which are given as follows.

TABLE V
PARAMETERS OF THE COIL STRUCTURES

	W_x (mm)	L_y (mm)	d_{sp} (mm)	d_1 (mm)	r_0 (mm)	Turn number	core	Strand number
Coil A	403.7	350	3.7	3.7	1.5	10	√	400
Coil B	403.7	350	3.7	3.7	1.5	10	√	300
Coil C	247.7	120	3.7	3.7	1.5	10	√	400
Coil D	263.7	230	3.7	3.7	1.5	10	√	300
Coil E	263.7	230	3.7	3.7	1.5	10	√	400
Coil F	403.7	350	3.7	3.7	1.5	10	×	400
Coil G	403.7	350	3.7	3.7	1.5	10	×	300
Coil H	247.7	120	3.7	3.7	1.5	10	×	400
Coil I	403.7	350	5	5	1.5	4	√	400
Coil K	403.7	350	5	5	1.5	6	√	400

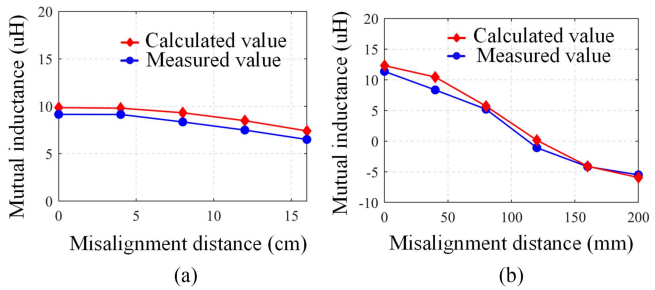

Fig. 25. Mutual inductance against the misalignment distance. (a) Coils on two sides have the same size as that of coil A, $h = 250$ mm. (b) Primary is coil A and secondary is coil C, $h = 150$ mm.

TABLE IV
SELF-INDUCTANCE OF THE DD COIL

	Coil A	Coil B	Coil C	Coil D
Calculated value	194 μH	39.4 μH	90.9 μH	30 μH
Experimental value	189.2 μH	38.1 μH	86 μH	29 μH

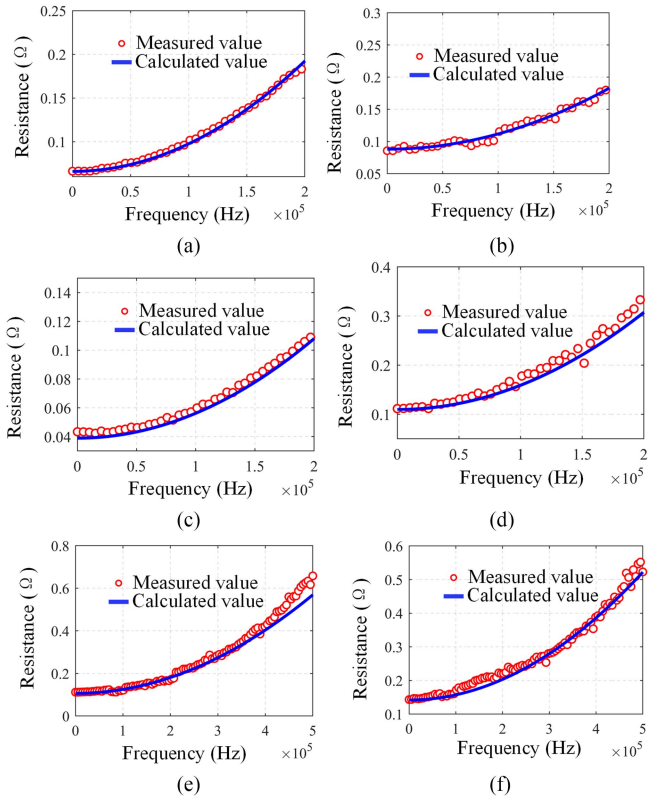

Fig. 26 AC resistance of the DD coil against the frequency. (a) Coil E. (b) Coil D. (c) Coil C. (d) Coil A. (e) Coil G. (f) Coil F.

1) When the quality factor is higher, the measurement accuracy of the instrument is harder to guarantee. The excitation current of the coil used for the measurement is smaller with higher frequency, which further increases the measurement error.
2) The resistance caused by the proximity effect is the most important part when it is high frequency. The impact of unideal twisting of Litz wire on the proximity effect will become more and more obvious.
3) The same coil with higher frequency, the larger error caused by the displacement current.

C. Coil Design and Experimental System Setup

When the WPT system operated at the resonant frequency, the coupler transfer efficiency increases with increasing the $k^2Q_1Q_2$ [50]. Q_1 and Q_2 are defined as the quality factors of the coils on the primary and secondary sides, respectively. The coupler maximum transfer efficiency can be calculated by

$$\eta = \frac{\sigma}{\left(1+\sqrt{1+\sigma}\right)^2}, \sigma = k^2Q_1Q_2$$

$$Q_1 = \frac{\omega L_{\mathrm{P}}}{R_{\mathrm{p}}}, Q_2 = \frac{\omega L_{\mathrm{s}}}{R_{\mathrm{s}}}. \tag{36}$$

For gaining the maximum value of $k^2Q_1Q_2$, the coupler can be optimized by sweeping a large number of coil structure parameters with the help of FEA software. However, this method is so time-consuming especially for solving the ac resistance of the coil. In this article, a genetic algorithm based on the proposed coil model is proposed to optimize the coil structure. The main structural parameters available for design are the outer dimension (W_{xp}, L_{yp}, W_{xs}, and L_{ys}), coil turn number (N_1 and N_2), the distance between the coil and ferrite core d_{fe}, and turn space (d_{sp}, d_{ss}). The outer dimension of the coil is decided by the available installation space. Therefore, coil turn number (N_1 and N_2), the distance between the coil and ferrite core d_{fe}, and turn space (d_{sp} and d_{ss}) are selected to optimize the coil. In this article, the coils on two sides are designed with the same structure. The Litz wire adopted is AWG-38 with 400 strands. The design flow chart is given in Fig. 27.

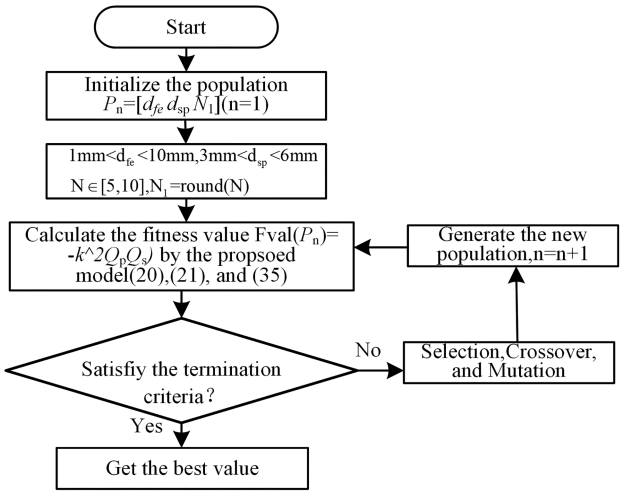

Fig. 27. Flowchart of the genetic algorithm.

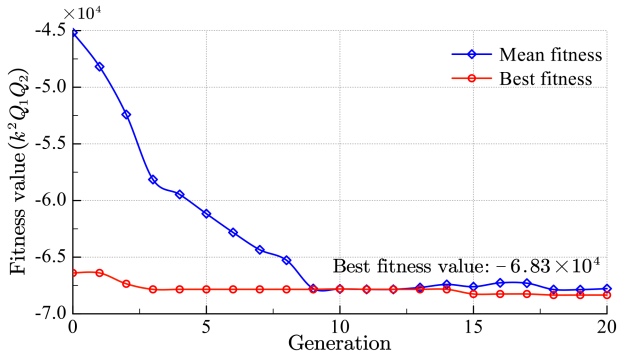

Fig. 28. Best fitness value ($k^2Q_1Q_2$) for each generation.

According to the genetic algorithm, the optimal parameters of the coils can be gained. The cputime of the algorithm only is 48 s, which significantly shortens the design time. The best fitness value ($k^2Q_1Q_2$) for each generation is given in Fig. 28. The coils number N_1 is 10. d_{fe} is 1.7 mm, and the d_{sp} is 3.7 mm, which are set as the main coil parameters.

The designed coil is shown in Fig. 23(d). The WPT system topology adopted in this article is shown in Fig. 1, which consists of a high-frequency inverter, a dual-sided *LCC* compensation network, and a high-frequency rectifier. S_1–S_4 and Q_1–Q_4 are the power switches of primary and secondary side converters, respectively. The output voltage v_{ab} of the inverter excites the resonant network. L_p and L_s are the primary and secondary coils used for transferring energy from the primary side to secondary

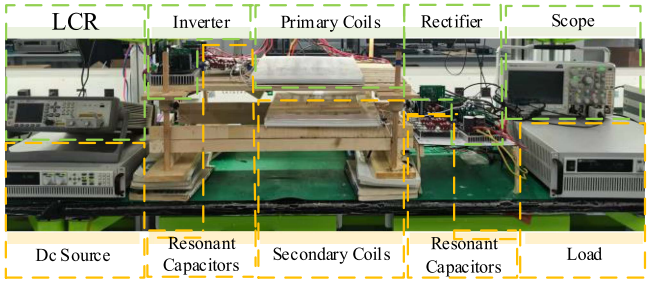

Fig. 29. Experiment prototype.

TABLE VI
EXPERIMENTAL PARAMETERS

Symbol	Value	Symbol	Value	Symbol	Value
L_p	194 μH	L_s	194 μH	L_{rp}	31 μH
L_{rs}	31 μH	R_{rp}	61 mΩ	R_{rs}	61 mΩ
R_s	160 mΩ	R_p	157 mΩ	V_{in}	100 V
R_L	10.5 Ω	k	0.27	f	85 kHz

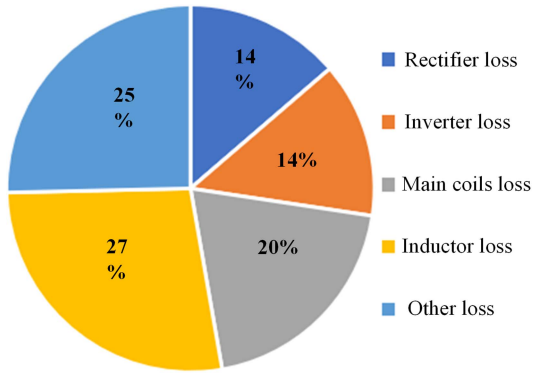

Fig. 30. Loss distribution of the system.

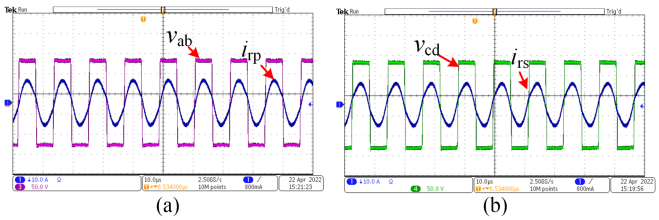

Fig. 31. Key waveforms of the system. (a) Current i_{ab} and voltage u_{ab}. (b) Current i_{cd} and voltage u_{cd}.

side. L_{rp} and L_{rs} are the compensation inductor. The C_{rp}, C_s, C_{rs}, and C_p are the resonant capacitors. v_{cd} is input voltage of rectifier that is converted into dc voltage V_o by the full-bridge rectifier. R_L represents the load resistance.

The experimental prototype is shown in Fig. 29. The experimental parameters are listed in Table VI.

The Mosfet used in the system is IXTQ96N20P. The system transfer efficiency achieves 94.5% with output power $P = 1152$ W. The operation frequency f is set 85 kHz. The key waveforms of the WPT system are given in Fig. 31. The power loss distribution is described in Fig. 30. It can be seen from Fig. 30 that the coil loss only accounts for 1.2% of the total input power. The designed coupler has high transfer efficiency.

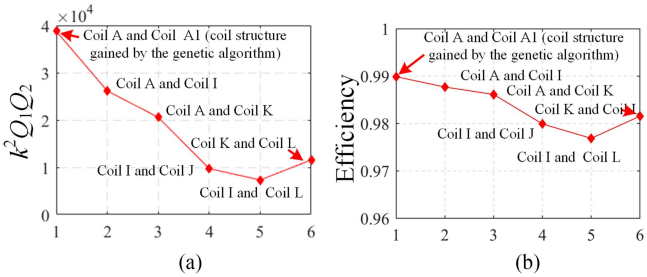

Fig. 32. Experimental results of different coil performance. (a) Value of $k^2Q_1Q_2$. (b) Coupler transfer efficiency.

For further verifying the fitness of the optimization method, several coils with different structure parameters were fabricated for comparison. The coil structure parameters are listed in the Table V. Experimental results are shown in Fig. 32. The coil $A1$, coil J, coil K has the same structure parameters as the coil A, coil I, and coil L. The value of $k^2Q_1Q_2$ is measured by the LCR HIOKI IM3536. The maximum transfer efficiency of coupler in Fig. 32(b) can be gained by (36).

From the results in Fig. 32, it can be seen the coil structure gained by the genetic algorithm has the best performance of the efficiency. This article just gives an example of applying the proposed model to optimize the efficiency of the coupler for showing the potential value of coil model.

VI. CONCLUSION

In this article, the theoretical model of a rectangular DD coil with ferrite core for calculating the self-inductance, mutual inductance, and ac resistance is proposed. The condition when there exist a misalignment is considered. Meanwhile, the size of coil on the primary side and secondary side is different and is also considered. Besides, a genetic algorithm based on the proposed coil mathematical model is proposed to optimize the coil structure. The cputime of the genetic algorithm for optimizing the coil structure is only 48 s.

For verifying the accuracy of the proposed model, the simulation model based on the FEA and a 1.2-kW laboratory prototype are built simultaneously. The analytically calculated value based on the proposed model is in good consistency with the simulation results and experimental values. Error for calculating the self-inductance and mutual inductance is within 5% when coils on primary and secondary sides are in alignment. The error for calculating the ac resistance of the coil is within 10% when the frequency range is 0–200 kHz. The system transfer efficiency achieves 94.5% with output power $P = 1152$ W. The coil loss only accounts for 1.2% of the total input power.

APPENDIX

According to (30) and Fig. 33, the $H_{ia\_j}(i = 1)$ can be calculated by

$$H_{1a\_j} = \sum_{k=1}^{N_1} \vec{H}(\Delta x_k, \Delta y_k, \Delta z_k)$$

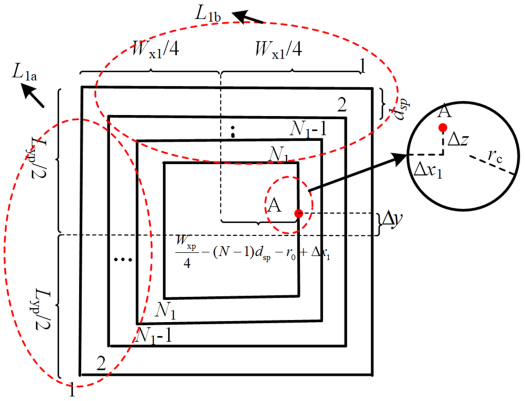

Fig. 33. Left half of the DD coil.

$$\Delta x_k = ((N+1-k)d_{sp}+W_{xp}/2-2(N-1)d_{sp}-r_c+\Delta x_1)$$
$$\Delta \mathrm{y}_k = \Delta \mathrm{y}, \Delta z_k = \Delta z \tag{37}$$

$$H_{1a1\_j} = \sum_{k=1}^{N_1} \overrightarrow{H}(\Delta x_{k1}, \Delta \mathrm{y}_{k1}, \Delta z_{k1})$$
$$\Delta x_k = ((N+1-k)d_{sp}+W_{xp}/2-2(N-1)d_{sp}-r_c+\Delta x_1)$$
$$\Delta \mathrm{y}_k = \Delta \mathrm{y}, \Delta z_k = \Delta z - 2d_{fe} \tag{38}$$

$$H_{1\mathrm{b}\_j} = \sum_{k=2}^{N_1} \overrightarrow{H}\,(\Delta x_k, \Delta \mathrm{y}_k, \Delta z_k)$$
$$\Delta y_k = ((W_{xp}/4 - (N_1-1)d_{sp} - r_c+\Delta x_1)\, d_{sp}$$
$$\Delta x_k = \frac{L_{yp}}{2} - \Delta \mathrm{y} - (k-1)d_{sp}, \Delta z_k = \Delta z \tag{39}$$

$$H_{1\mathrm{b}1\_j} = \sum_{k=1}^{N_1} \overrightarrow{H}(\Delta x_{k1}, \Delta \mathrm{y}_{k1}, \Delta z_{k1})$$
$$\Delta y_{k1} = ((W_{xp}/4 - (N_1-1)d_{sp} - r_c+\Delta x_1)\, d_{sp}$$
$$\Delta x_{k1} = \frac{L_{yp}}{2} - \Delta \mathrm{y} - (k-1)d_{sp}, \Delta z_{k1} = \Delta z - 2d_{\mathrm{fe}} \tag{40}$$

where $H_{i\mathrm{a}}$, $H_{i\mathrm{b}}$, $H_{i\mathrm{a}1}$, and $H_{i\mathrm{b}1} (i = 2, 3, 4)$ can be calculated by a method similar to (33)–(36).

REFERENCES

[1] S. Stoecklin, A. Yousaf, T. Volk, and L. Reindl, "Efficient wireless powering of biomedical sensor systems for multichannel brain implants," *IEEE Trans. Instrum. Meas.*, vol. 65, no. 4, pp. 754–764, Apr. 2016.

[2] Y. Jiang et al., "Phase-locked loop combined with chained trigger mode used for impedance matching in wireless high power transfer," *IEEE Trans. Power Electron.*, vol. 35, no. 4, pp. 4272–4285, Apr. 2020, doi: 10.1109/TPEL.2019.2936708.

[3] M. Wu et al., "A dual-sided control strategy based on mode switching for efficiency optimization in wireless power transfer system," *IEEE Trans. Power Electron.*, vol. 36, no. 8, pp. 8835–8848, Aug. 2021, doi: 10.1109/TPEL.2021.3055963.

[4] M. Wu et al., "A compact coupler with integrated multiple decoupled coils for wireless power transfer system and its anti-misalignment control," *IEEE Trans. Power Electron.*, vol. 37, no. 10, pp. 12814–12827, Oct. 2022, doi: 10.1109/TPEL.2022.3166888.

[5] Y. Jiang, L. Wang, Y. Wang, J. Liu, M. Wu, and G. Ning, "Analysis, design, and implementation of WPT system for EV's battery charging based on optimal operation frequency range," *IEEE Trans. Power Electron.*, vol. 34, no. 7, pp. 6890–6905, Jul. 2019, doi: 10.1109/TPEL.2018.2873222.

[6] A. Askari, R. Stark, J. Curran, D. Rule, and K. Lin, "Underwater wirelesspower transfer," in *Proc. IEEE Wirel. Power Transfer Conf.*, 2015,pp. 1–4.

[7] H. Lee, H. Park, and M. Ghovanloo, "A power-efficient wireless system with adaptive supply control for deep brain stimulation," *IEEE J. Solid-State Circuits*, vol. 48, no. 9, pp. 2203–2216, Sep. 2013.

[8] M. Budhia, J. T. Boys, G. A. Covic, and C.-Y. Huang, "Development of a single-sided flux magnetic coupler for electric vehicle IPT charging systems," *IEEE Trans. Ind. Electron.*, vol. 60, no. 1, pp. 318–328, Jan. 2013, doi: 10.1109/TIE.2011.2179274.

[9] R. Schlesinger and J. Biela, "Comparison of analytical models of transformer leakage inductance: Accuracy versus computational effort," *IEEE Trans. Power Electron.*, vol. 36, no. 1, pp. 146–156, Jan. 2021, doi: 10.1109/TPEL.2020.3001056.

[10] A. Zaheer, H. Hao, G. A. Covic, and D. Kacprzak, "Investigation of multiple decoupled coil primary pad topologies in lumped IPT systems for interoperable electric vehicle charging," *IEEE Trans. Power Electron.*, vol. 30, no. 4, pp. 1937–1955, Apr. 2015, doi: 10.1109/TPEL.2014.2329693.

[11] G. Yang et al., "Interoperability improvement for rectangular pad and DD pad of wireless electric vehicle charging system based on adaptive position adjustment," *IEEE Trans. Ind. Appl.*, vol. 57, no. 3, pp. 2613–2624, May/Jun. 2021, doi: 10.1109/TIA.2021.3056639.

[12] F. Wen, X. Cheng, Q. Li, W. Zhao, X. Zhu, and Y. Wu, "A strong misalignment tolerance dual-channel coupler for wireless power transfer system," *IEEE Trans. Appl. Supercond.*, vol. 31, no. 8, Nov. 2021, Art. no. 0601005, doi: 10.1109/TASC.2021.3091099.

[13] M. E. Bima, I. Bhattacharya, and C. W. V. Neste, "Experimental evaluation of layered DD coil structure in a wireless power transfer system," *IEEE Trans. Electromagn. Compat.*, vol. 62, no. 4, pp. 1477–1484, Aug. 2020, doi: 10.1109/TEMC.2020.3002694.

[14] M. Mohammad, S. Choi, and M. E. Elbuluk, "Loss minimization design of ferrite core in a DD-coil-based high-power wireless charging system for electrical vehicle application," *IEEE Trans. Transp. Electrific.*, vol. 5, no. 4, pp. 957–967, Dec. 2019, doi: 10.1109/TTE.2019.2940878.

[15] H. Pang, K. T. Chau, W. Han, W. Liu, and Z. Zhang, "Decoupled-double D coils based dual-resonating-frequency compensation topology for wireless power transfer," *IEEE Trans. Magn.*, vol. 58, no. 2, Feb. 2022, Art. no. 8000407, doi: 10.1109/TMAG.2021.3091456.

[16] H. A. Wheeler, "Inductance formulas for circular and square coils," *Proc. IEEE*, vol. 70, no. 12, pp. 1449–1450, Dec. 1982.

[17] M. T. Thompson, "Inductance calculation techniques—Part II: Approximations and handbook methods," *Power Control Intell. Motion*, vol. 25, no. 12, pp. 40–50, 1991.

[18] W. G. Hurley and M. C. Duffy, "Calculation of self and mutual impedances in planar magnetic structures," *IEEE Trans. Magn.*, vol. 31, no. 4, pp. 2416–2422, Jul. 1995, doi: 10.1109/20.390151.

[19] W. G. Hurley and M. C. Duffy, "Calculation of self- and mutual impedances in planar sandwich inductors," *IEEE Trans. Magn.*, vol. 33, no. 3, pp. 2282–2290, May 1997, doi: 10.1109/20.573844.

[20] M. Soma, D. C. Galbraith, and R. L. White, "Radio-frequency coils in implantable devices: Misalignment analysis and design procedure," *IEEE Trans. Biomed. Eng.*, vol. BME-34, no. 4, pp. 276–282, Apr. 1987.

[21] F. J. López-Alcolea, J. V.D. Real, P. Roncero-Sánchez, and A. P. Torres, "Modeling of a magnetic coupler based on single- and double-layered rectangular planar coils with in-plane misalignment for wireless power transfer," *IEEE Trans. Power Electron.*, vol. 35, no. 5, pp. 5102–5121, May 2020.

[22] A. K. RamRakhyani, S. Mirabbasi, and M. Chiao, "Design and optimization of resonance-based efficient wireless power delivery systems for biomedical implants," *IEEE Trans. Biomed. Circuits Syst.*, vol. 5, no. 1, pp. 48–63, Feb. 2011, doi: 10.1109/TBCAS.2010.2072782.

[23] S. Raju, R. Wu, M. Chan, and C. P. Yue, "Modeling of mutual coupling between planar inductors in wireless power applications," *IEEE Trans. Power Electron.*, vol. 29, no. 1, pp. 481–490, Jan. 2014, doi: 10.1109/TPEL.2013.2253334.

[24] S. R. Khan, S. K. Pavuluri, and M. P. Y. Desmulliez, "Accurate modeling of coil inductance for near-field wireless power transfer," *IEEE Trans. Microw. Theory Techn.*, vol. 66, no. 9, pp. 4158–4169, Sep. 2018, doi: 10.1109/TMTT.2018.2854190.

[25] B. K. Kushwaha, G. Rituraj, and P. Kumar, "3-D Analytical model for computation of mutual inductance for different misalignments with shielding in wireless power transfer system," *IEEE Trans. Transp. Electrific.*, vol. 3, no. 2, pp. 332–342, Jun. 2017, doi: 10.1109/TTE.2017.2649881.
[26] Z. Luo and X. Wei, "Analysis of square and circular planar spiral coils in wireless power transfer system for electric vehicles," *IEEE Trans. Ind. Electron.*, vol. 65, no. 1, pp. 331–341, Jan. 2018.
[27] S. R. Khan and M. Desmulliez, "Design and manufacture of a 3-D WPT coil for capsule endoscopy," 2017.
[28] S. R. Khan, S. K. Pavuluri, G. Cummins, and M. P. Y. Desmulliez, "Miniaturized 3-D cross-type receiver for wirelessly powered capsule endoscopy," *IEEE Trans. Microw. Theory Techn.*, vol. 67, no. 5, pp. 1985–1993, May 2019, doi: 10.1109/TMTT.2019.2893204.
[29] P. T. Theilmann and P. M. Asbeck, "An analytical model for inductively coupled implantable biomedical devices with ferrite rods," *IEEE Trans. Biomed. Circuits Syst.*, vol. 3, no. 1, pp. 43–52, Feb. 2009, doi: 10.1109/TBCAS.2008.2004776.
[30] A. Sharma and J. W. Kimball, "Evaluation of transformer leakage inductance using magnetic image method," *IEEE Trans. Magn.*, vol. 57, no. 11, Nov. 2021, Art no. 8401912, doi: 10.1109/TMAG.2021.3111479.
[31] M. Eslamian, M. Kharezy, and T. Thiringer, "An accurate method for leakage inductance calculation of shell-type multi core-segment transformers with circular windings," *IEEE Access*, vol. 9, pp. 111417–111431, 2021, doi: 10.1109/ACCESS.2021.3103541.
[32] X. Yan, W. Zengping, and L. Qing, "A novel inductance calculation method in power transformer model based on magnetic circuit," in *Proc. IEEE Region 10 Conf.*, 2005, pp. 1–4, doi: 10.1109/TENCON.2005.301303.
[33] M. Akbari, A. Rezaei-Zare, M. A. M. Cheema, and T. Kalicki, "Air gap inductance calculation for transformer transient model," *IEEE Trans. Power Del.*, vol. 36, no. 1, pp. 492–494, Feb. 2021, doi: 10.1109/TEC.2020.3009818.
[34] J. Acero, R. Alonso, J. M. Burdio, L. A. Barragan, and D. Puyal, "Frequency-dependent resistance in Litz-wire planar windings for domestic induction heating appliances," *IEEE Trans. Power Electron.*, vol. 21, no. 4, pp. 856–866, Jul. 2006.
[35] J. Acero, C. Carretero, R. Alonso, and J. M. Burdío, "Quantitative evaluation of induction efficiency in domestic induction heating applications," *IEEE Trans. Magn.*, vol. 49, no. 4, pp. 1382–1389, Apr. 2013.
[36] C. Carretero, J. Acero, and R. Alonso, "TM-TE decomposition of power losses in multi-stranded Litz-wires used in electronic devices," *Prog. Electromagn. Res.*, vol. 123, pp. 83–103, Jan. 2012.
[37] M. Lu and K. D. T. Ngo, "Analytical calculation of proximity-effect resistance for planar coil with Litz wire and ferrite plate in inductive power transfer," *IEEE Trans. Ind. Appl.*, vol. 55, no. 3, pp. 2984–2991, May/Jun. 2019, doi: 10.1109/TIA.2018.2890366.
[38] X. Nan and C. R. Sullivan, "Simplified high-accuracy calculation of eddycurrent loss in round-wire windings," in *Proc. IEEE Power Electron. Specialists Conf.*, 2004, pp. 873–879.
[39] P. L. Dowell, "Effects of eddy currents in transformer windings," *Proc. Inst. Elect. Eng.*, vol. 113, no. 8, pp. 1387–1394, Aug. 1966.
[40] C. R. Sullivan, "Optimal choice for number of strands in a Litz-wire transformer winding," *IEEE Trans. Power Electron.*, vol. 14, no. 2, pp. 283–291, Mar. 1999.
[41] R. P. Wojda and M. K. Kazimierczuk, "Winding resistance of Litz-wire and multi-strand inductors," *IET Power Electron.*, vol. 5, no. 2, pp. 257–268, Feb. 2012.
[42] C. Carretero, I. Lope, R. Alonso, and J. M. Burdio, "FEA-based model of elliptic coils of square cross section," *IEEE Trans. Magn.*, vol. 50, no. 7, Feb. 2014, Art. no. 8401107.
[43] A. Rosskopf, E. Bar, and C. Joffe, "Influence of inner skin- and proximity effects on conduction in Litz wires," *IEEE Trans. Power Electron.*, vol. 29, no. 10, pp. 5454–5461, Oct. 2014.
[44] E. B. Rosa, "The self and mutual inductances of linear conductors," *Bull. Bur. Standards*, vol. 4, no. 2, pp. 301–344, 1908.
[45] F. W. Grover, *Inductance Calculations*. New York, NY, USA: Van Nostrand, 1946.
[46] A. Zisserman, R. Saunders, and J. Caldwell, "Analytic solutions for axisymmetric magnetostatic systems involving iron," *IEEE Trans. Magn.*, vol. 23, no. 6, pp. 3895–3902, Nov. 1987, doi: 10.1109/TMAG.1987.1065773.
[47] M. Lambert, F. Sirois, M. Martinez-Duro, and J. Mahseredjian, "Analytical calculation of leakage inductance for low-frequency transformer modeling," *IEEE Trans. Power Del.*, vol. 28, no. 1, pp. 507–515, Jan. 2013, doi: 10.1109/TPWRD.2012.2225451.
[48] J. A. Ferreira, *Electromagnetic Modelling of Power Electronics Converters*. Norwell, MA, USA: Kluwer, 1989.
[49] C. R. Sullivan and R. Y. Zhang, "Analytical model for effects of twisting on Litz-wire losses," in *Proc. IEEE 15th Workshop Control Model. Power Electron.*, 2014, pp. 1–10, doi: 10.1109/COMPEL.2014.6877187.
[50] Y. Zhang, Z. Zhao, and K. Chen, "Frequency decrease analysis of resonant wireless power transfer," *IEEE Trans. Power Electron.*, vol. 29, no. 3, pp. 1058–1063, Mar. 2014.

Min Wu was born in Sichuan, China, in 1995. He received the B.S. degree in electrical automatization from Chongqing University, Chongqing, China, in 2017. He is currently working toward the Ph.D. degree in electrical engineering and automation with Xi'an Jiaotong University, Xi'an, China.

His research interest is wireless power transfer and high-frequency power converter.

Xu Yang (Senior Member, IEEE) received the B.S. and Ph.D. degrees in electrical engineering from Xi'an Jiaotong University, Xi'an, China, in 1994 and 1999, respectively.

Since 1999, he has been a Member with the Faculty of School of Electrical Engineering, Xi'an Jiaotong University, where he is currently a Professor. From November 2004 to November 2005, he was with the Center of Power Electronics Systems (CPES), Virginia Polytechnic Institute and State University, Blacksburg, VA, USA, as a Visiting Scholar. He then came back to Xi'an Jiaotong University, and engaged in the teaching and researches in power electronics and industrial automation area. His research interests include soft switching topologies, PWM control techniques, electromagnetic compatibility power electronic integration, and packaging technologies.

Hongchang Cui (Graduate Student Member, IEEE) was born in Shanxi, China, in 1999. He received the B.S. degree in electrical engineering from the China University of Mining and Technology, Xuzhou, China, in 2021. He is currently working toward the M.S. degree in electrical engineering with Xi'an Jiaotong University, Xi'an, China.

His current research interests include packaging, advanced thermal management of power modules, and wireless power transfer.

Wenjie Chen (Senior Member, IEEE) received the B.Sc., M.Sc., and Ph.D. degrees in electrical engineering from Xi'an Jiaotong University, Xi'an, China, in 1996, 2002, and 2006, respectively.

Since 2002, she has been a Member of the Faculty of School of Electrical Engineering, Xi'an Jiaotong University, where she is currently a Professor. From January 2012 to January 2013, she was with the Department of Electrical Engineering and Computer Science, University of Tennessee, Knoxville, TN, USA, as a Visiting Scholar. She then came back to Xi'an Jiaotong University, and engaged in the teaching and researches in power electronics. Her research interests include electromagnetic interference, active filters, and power electronic integration.

Laili Wang (Senior Member, IEEE) was born in Shaanxi, China, in 1982. He received the B.S., M.S., and Ph.D. degrees in electrical engineering from Xi'an Jiaotong University, Xi'an, China, in 2004, 2007, and 2011, respectively.

Since 2011, he has been a Postdoctoral Research Fellow with the Department of Electrical Engineering, Queen's University, Kingston, ON, Canada. From 2014 to 2017, he was an Electrical Engineer with Sumida, Mississauga, ON, Canada. In 2017, he joined Xi'an Jiaotong University as a Professor. His research interests include package and integration of passive devices in high-frequency high power density dc–dc converters, wireless power transfer, and energy harvesting.

Lei Zhu (Graduate Student Member, IEEE) was born in Anhui, China, in 1995. She received the B.S. degree in electrical engineering from Xi'an Jiaotong University, Xi'an, China, in 2018. she is currently working toward the Ph.D. degree in electrical engineering and automation with Xi'an Jiaotong University, Xi'an, China.

Her research interests include wireless power transfer, high frequency, and high power density dc–dc converters, signal processing, and digital control technology.

Xipei Yu received the B.S. degree in electrical engineering from Xi'an Jiaotong University, Xi'an, China, in 2021. He is currently working toward the Ph.D. degree with the Center for Power Electronics Systems, Virginia Tech, Blacksburg, VA, USA.

His research interests include high-frequency power conversion, wireless power transfer, and resonant converters.

Zhengchao Yan (Member, IEEE) received the B.S. and Ph.D. degrees in electrical engineering from Northwestern Polytechnical University, Xi'an, China, in 2013 and 2020, respectively.

From 2017 to 2019, he was a Joint Ph.D. Student with the San Diego State University, San Diego, CA, USA. Since 2020, he has been an Assistant Professor with the School of Electrical Engineering, Xi'an Jiaotong University, Xi'an, China. His research focuses on wireless power transfer, including electromagnetic field calculation, coil design, and compensation topologies.